Chapter 5

Atomization and Granulation

Oleg D. Neikov, Frantsevich Institute for Problems of Materials Science (IPMS), Kiev, Ukraine

Because of the ease with which a liquid can be broken up into fine droplets, atomization has become the prevailing mode of powder production of non-ferrous metals and their alloys. Currently, the world-wide atomization capacity of non-ferrous metals amounts to 10 million metric tonnes per year [1]. Atomization allows the manufacture of rapidly solidified metal alloys. The use of rapid solidification of melts to produce new structural and other materials with complex properties unachievable by traditional metallurgy is not only a very popular subject of investigation but also finds a wide industrial application nowadays.

The basic types of atomization processes include (Figure 5.1):

- Jet atomization of the melt, where a liquid metal is dispersed into droplets by the impingement of high-pressure jets of gas, water or oil (Figure 5.1(a) and (b))
- Centrifugal atomization, where a liquid stream is dispersed into droplets, flakes, or ribbons by the centrifugal force effect of a rotating disk, spinning cup, spinning roller or consumable electrode (Figure 5.1(c))
- Disintegration of liquid metal (Figure 5.1(d))
- Impact atomization a liquid stream (Figure 5.1(e))
- Ultrasonic atomization, where a liquid metal film is subjected to ultrasonic vibration (Figure 5.1(f))
- Impulse atomization, where impulses are mechanically applied to the melt (Figure 5.1(g))
- Vacuum atomization, where heavily saturated molten metal with a gas is atomized in the vacuum (Figure 5.1(h)).

Particle size distribution is one of the most important parameters of powders. The particle size distribution of atomized powders generally follows the log normal law. This signifies that the particle size distributions form straight or nearly straight lines on the log-probability paper (Figure 5.2).

Granulation of a melt is realized by means of free fall into cold liquid, usually water. During the free fall and by impact with the water surface, the melt stream is broken up into droplets which then solidify. The melt is caused to flow through a nozzle plate (see Figure 5.1(g)) in order to obtain granules of pellet shape. Particulate materials coarser than 1 mm in diameter are conventionally referred to as granules (see Introduction). Thus, several types of conventional atomization processes are useful for granule production.

Water Atomization

Water atomization (WA) is used for commercial production of copper, copper alloys, nickel-base alloys and zinc powders. Water atomized precious metals are used in dental techniques, sintered electrical contacts and brazing pastes. WA is less expensive than other methods of atomization. It allows the production of powders within wide yield limits from 1 to 500 kg/min for a single nozzle. The main limitation of WA is powder purity, especially for metals and alloys inclined to oxidation. However, owing to the higher cooling rate of the melt by WA, the average thickness of surface oxides is similar to that in gas atomized powders. This is realized, in particular, in water atomized aluminum alloys [4] (discussed in Chapter 13).

Technique

The major components of a conventional water atomization system are a melting unit, a tundish, an atomizing chamber, a water pumping/recycling system, and the dewatering and drying units. A flow diagram of the typical water atomization process for copper and copper alloy powders production is shown in Chapter 16.

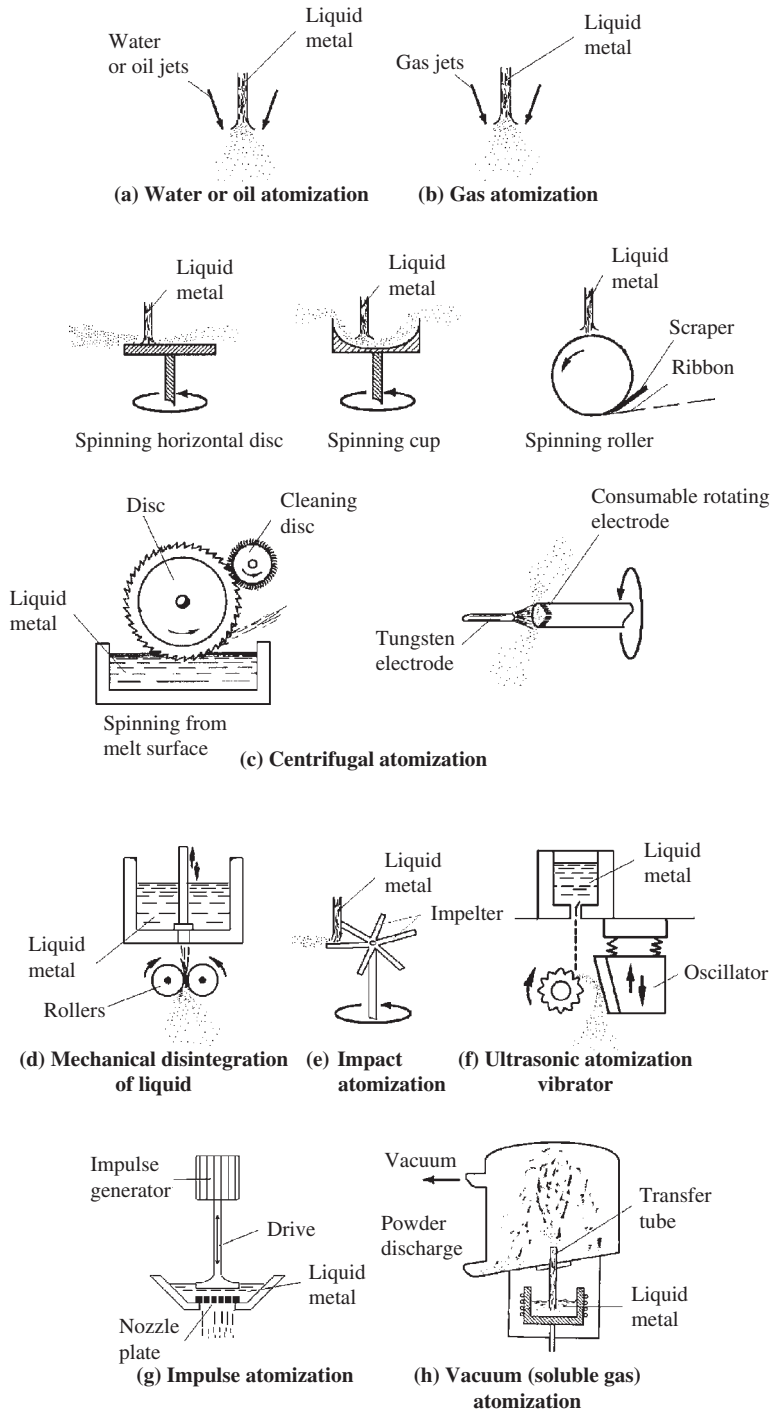

Figure 5.1 Schematic drawing of atomization processes.

Conventional installations usually operate with water pressure in the region of 5–20 MPa, producing the powders with mass median particle sizes of 30–50 μm. Significantly higher water pressures of 50–150 MPa are used to manufacture finer powders with mass median particles sizes of 1–20 μm. These powders are used for injection molding processes, binders in diamond tools, sintered bearings, paints, coatings and pastes.

Generally, the water atomizer designs are based on 'V' configurations with some nozzles (at the minimum two) located symmetrically about the axis of the liquid metal stream (Figure 5.3).

A representation of the overall processing stages in water atomization is shown in Figure 5.3. The associated melting process variables include the charge ingredients, atmosphere and superheat of the melt; the associated atomization stage variables are nozzle

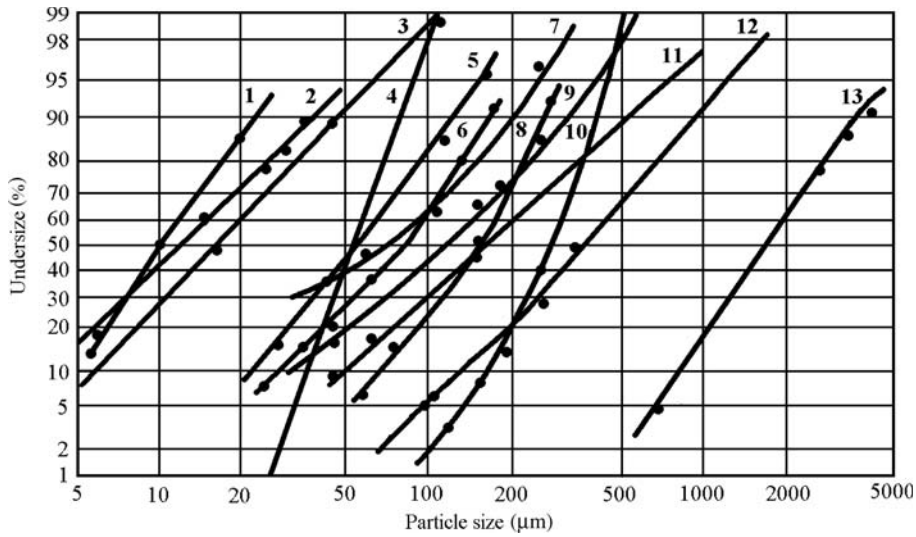

Figure 5.2 Typical particle size distribution of atomized powders.

Curve No	Powder	Median mass diameter (d_m), μm	Geometric standard deviation (σ_g)	Ref
1	Copper, hot-gas atomized at 4.5 MPa in nitrogen at 500°C	10	2.0	(Ref 2)
2	Copper, water atomized at 54 MPa	12.5	2.4	(Ref 3)
3	Zinc, gas atomized at 2 MPa	16	2.1	(Ref 3)
4	67Pb-33Sn ultrasonically atomized	64	1.31	(Ref 3)
5	44.85Al-13.7Fe-28.55Cu-12.9Cr, water atomized at 10 MPa	55	1.83	A*
6	43Al-40Cu17Fe, argon atomized at 0.6 MPa	87	2.48	–
7	60Pb-40Sn solder, gas atomized at 0.8 MPa	70	2.5	(Ref 3)
8	Aluminum, water atomized at 4.8 MPa	150	2.0	A*
9	Bronze, air atomized at 0.5 MPa	120	2.33	(Ref 3)
10	Zinc, centrifugally atomized	270	1.4	(Ref 3)
11	Zinc, water atomized at 5.5 MPa	170	2.58	(Ref 3)
12	Copper shot, water atomized at 2 MPa	280	2.1	(Ref3)
13	Phosphor shot, water atomized at 0.05 MPa	1950	1.9	(Ref 3)

A*, author's data have first been published

diameter, metal stream length, density of metal, surface tension of the melt, viscosity of the melt, water pressure, jet geometry and apex angle; key variables in the particle solidification stage are melting point, droplet size, heat transfer, quenching medium, temperature of suspended solid in atomization chamber and flight path. Basic water-jet configurations are shown in Figure 5.4.

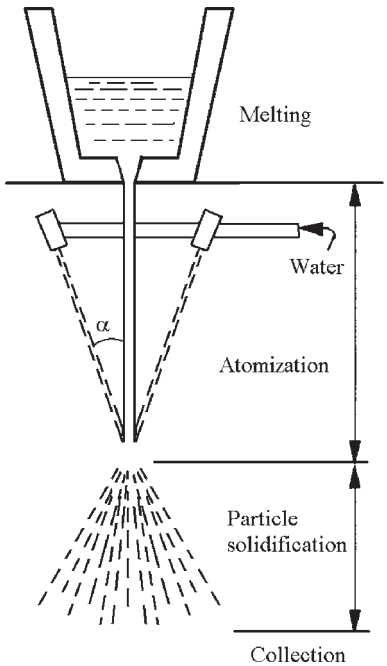

Figure 5.3 Stages in water atomization.

Typical range of operating conditions in water atomization are as follows [3]:

- Metal flow rate (single nozzle), 1–90 kg/min
- Water flow rate, 20–380 L/min
- Water velocity (at nozzle exit), 10–500 m/s
- Water pressure (at exit or in manifold), 5–150 MPa
- Metal superheat, 75–170 (above melting point).

Commercial water atomization plants typically operate with water flow to metal flow ratios between 2/1 and 15/1. Table 5.1 comprises the operating conditions for specific powders and their properties.

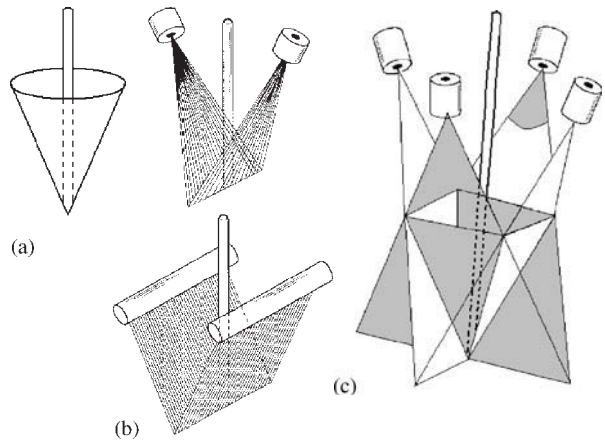

Figure 5.4 Water jet configurations: (a) annular jet; (b) open V-jets; (c) closed V-jets.

Table 5.1 Properties of several water-atomized powders

Alloy	Operating parameters				Powder properties		
	Metal flow (M) (kg/min)	Water flow (W) (L/min)	W/M ratio	Water pressure (MPa)	Median diameter r (μm)	Apparent density (g/mL)	Oxygen (ppm)
Ag (a)	18	100	5.5	50	21	3.4 (c)	...
Al-5Zn-3Mg-0.49Fe (b)	6.5	90	13.8	10	60	0.9 (d)	...
Al-1.3F-1.5Cr (b)	7.0	90	12.8	15	45	0.98 (d)	600
Cu-5Cr (a)	27	180	6.7	20	24	3.18 (c)	...
Co (a)	27	180	6.7	20	29	3.28 (c)	...
Au-2Cu (a)	7	40	5.7	13.7	88	...	...
Ag-22Cu-3Zn (a)	9	42	4.7	17.2	72	3.95 (c)	110
Ni-B-Si (a)	24	160	6.7	17.2	51	4.26 (c)	...

[a]All data from V-jet atomizer with 40–50 degrees apex angle, nitrogen purged;
[b]IPMS atomizer equipped with eight discrete nozzles;
[c]apparent density for fractions under size 250 μm;
[d]apparent density for fractions under size 63 μm;
(a) and (c) Source: Ref 3; (b) and (d) Source: IPMS

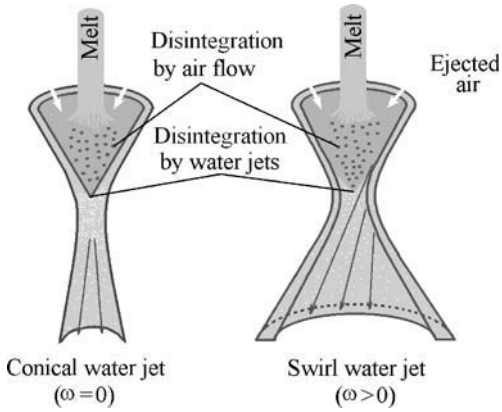

Figure 5.5 High-pressure water atomization using conical swirl water jet.

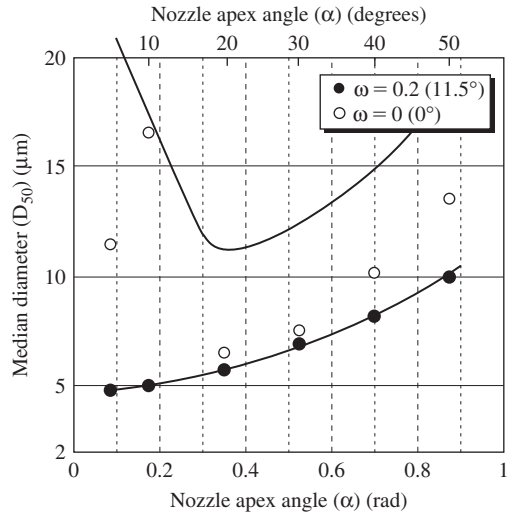

Figure 5.6 Dependence of powder median diameter on jet apex angle of conical swirl water jet atomizer.

Atomizer

The atomizers play the main role in ensuring the efficiency of the disintegration of a liquid metal stream. In the literature on atomization, the terms nozzles and jets are often used interchangeably. The jet is the stream of liquid or gas that flows out from the nozzle, whereas a nozzle is one part of the atomizer. As far as possible, the use of these terms throughout the book is consistent with these definitions.

Though numerous patents of atomizer design have been filed, only a few types of atomizer are used in most commercial water atomization units. Atomizer design in most commercial water atomization units are variants of either V-jet nozzles (see Figure 5.4) or annular cone-jet nozzles that are concentric with the metal stream. Annular ring nozzles are utilized in some large-capacity plants, but are rarely used elsewhere because they are less flexible and harder to make than designs based on V-nozzle configurations with two or more discrete openings located symmetrically about the axis defined by the metal stream.

The liquid metal stream typically falls a certain distance (usually about 15–25 cm) before meeting the water jets. A partial vacuum is often created above the impingement point with the water and the gas/air sucked by the water streams can disrupt the liquid metal before it actually meets the water jets [5].

A swirl water atomizer for fine powder production has been developed [6]. Figure 5.5 shows a schematic of high-pressure water atomization by 'free fall' design and swirl water jet. This unit allows the production of bronze (Cu–10 mass% Sn) powder with median particle size 7.5 μm and apparent density 2.8 g/cm^3 with water pressure of 83.3 MPa.

Figure 5.6 shows the effect of the jet configuration apex angle (θ) on the median diameter of swirl water atomized copper powder (δ_{50}) [7]. The water jets are generated at water pressure 90 MPa with flow rate 5 l/s on the jet swirl angle, $\omega = 0.2$ rad (≈11.5 degrees) and $\omega = 0.0$ rad (0.0 degrees), i.e. usual conical jet configuration. For $\omega = 0.0$ rad, δ_{50} of common conical jet configuration atomized powders decreases with decreasing θ down to 0.35 rad, but as θ becomes less than 0.35 rad, δ_{50} increases abruptly with decreasing θ, while, by swirl jet configuration for $\omega = 0.2$ rad, δ_{50} keeps decreasing with θ decreasing. As can be seen from dependences of δ_{50} on θ in the range $\theta = 0.35$ to $\theta = 0.87$ rad, δ_{50} for swirl jet configuration is less than one order of magnitude in comparison with common conical jet configuration. Via the latter, there are many coarse particles with wide size distribution (Figure 5.7). The particles are spherical or drip shaped, but with increasing θ up to 0.87 (≈50 degrees) the powders become irregular in shape. In the former, there are few irregular aggregates. Almost all particles were spherical and particle sizes decreased with decreasing θ.

Applications for such ultrafine powders include metal injection molding (MIM), sintered filters, conductive pastes and corrosion-resistant paints.

In atomization installations using an atomizer with a binary water cone configuration (Figure 5.8) [8], a second convergent water cone performing angular motion relative to the melt stream axis affects the atomized melt droplets. The lower annular nozzle is provided with tangential channels at 27–29 degrees that create swirl jet configuration. The apex angle of the upper nozzle ranges from 54 to 58 degrees and

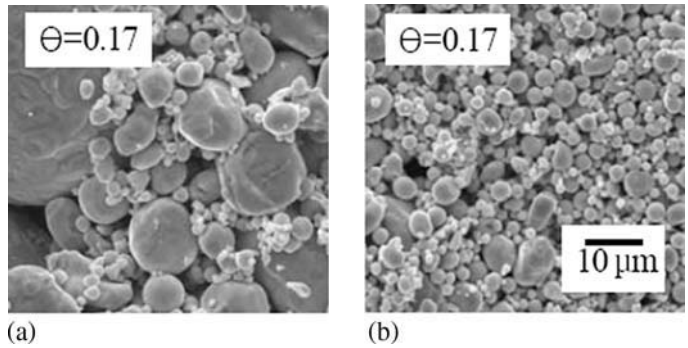

Figure 5.7 SEM micrographs of copper powders produced by the high-pressure water atomization using conical swirl water jet with apex angle 0.17 rad (≈9.7 degrees) and jet swirl angle, ω = 0 (a) i.e. common cone water jet configuration, and ω≈50 degrees (b), accordingly.

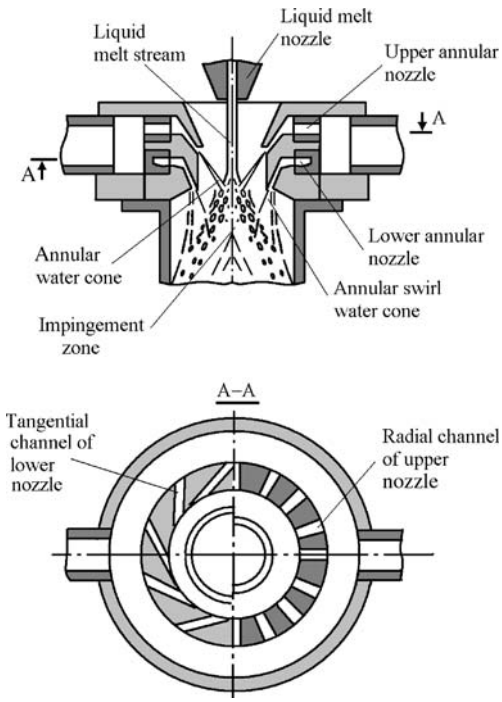

Figure 5.8 Atomizer with binary water cone configuration.

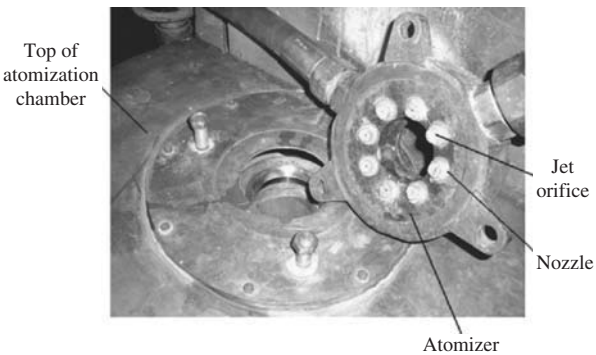

Figure 5.9 IPMS atomizer equipped with eight discrete nozzles. Courtesy of IPMS.

the lower one ranges from 36 to 40 degrees. The liquid melt outflow orifice is 9 mm.

The IPMS atomizer is equipped with eight discrete nozzles located symmetrically about the axis defined by the metal stream (Figure 5.9), four nozzles create closed V-jet configuration and disintegrate the metal stream on meeting the atomizing fluid. A second closed V-jet configuration is created by means of four nozzles that impinge on the melt stream at a more acute apex angle than the former. Thus, they meet the melt droplets after the impingement point.

Atomization Mechanism

The water-atomization process is distinguished by high density of the energy carrier, high cooling rate and steam formation in the contact zone between water and melt. High water density $\rho_{H_2O} \approx 10^3 \rho_{air}$ leads to an essential increase of impulse linear momentum $(p = mv)$ and kinetic energy $(E_k = mv^2/2)$ of the energy carrier.

Steam film originating around a drop decreases the heat transfer from drop to surroundings; if the film is disrupted and the contact of melt with water is provided, the cooling rate is appreciably accelerated. The high density of the energy carrier preserves the high velocity of water jets over a long distance that allows a wide range of positional relationships of melt streams and water jets and simplifies the design of hydraulic atomizers.

Liquid metal drops are disintegrated by a superheated compressed steam, which is formed on melt contact surface with water. The breakdown force of the steam film on the melt drop depends on the

physical conditions in the contact zone: temperature and density of steam as well as water pressure and volume.

The mechanism of liquid melt drop formation under the impact from the exploding water–steam packet rather than shear was first proposed by Grandzol and Tallmadge for water atomization [9]. This model reflects the dispersed nature of the water and an inverse proportionality between particle size and the normal velocity component of the water, with respect to the metal stream axis. Grandzol and Tallmadge represent the dependence of mass median particle size (δ_m) on the water drop velocity (v_w) such that:

$$\delta_m = \frac{A}{v_w} = \frac{14,900}{v_w}\left(\frac{1}{n}\right)^{1/3} \quad (1)$$

where A is a constant, δ_m is in μm, v_w is in m/s, and n is the number of metal droplets formed from the disintegration of one water droplet. In this equation, water flow rate, water pressure, momentum and energy, jet length and metal flow are not primary parameters influencing δ_m; they do, however, affect particle size by influencing water-jet velocities and the number of water droplets. Impingements during atomization can also influence particle size, particle size distribution and particle shape [10].

From subsequent experimental observations on the influence of the angle between the metal stream axis and the water jet axis on δ_m, it was concluded that the velocity component of the water normal to the liquid metal stream, rather than the velocity component parallel to the liquid metal stream, is the dominant parameter in controlling δ_m [11]. Thus, the refined model [12] gives a relation between δ_m and v_w of:

$$\delta_m = \frac{B}{v_w}\sin\alpha \quad (2)$$

where δ_m is in μm, v_w is in m/s, α is the angle (in degrees) between the axis of the metal stream and the water jets, and B is a constant. The value of B in conditions of the refined model [12] is 2750.

The relation between δ_m and water pressure (p_w) for various metal powders [13] is shown in Figure 5.10.

Based on the straight log–log plots in Figure 5.10, the relationship between δ_w and p_w can be expressed:

$$\delta_m = Kp_w^{-m} \quad (3)$$

where K and m are constants for a given material and atomization unit. For atomizer modification with two nozzles, when δ_m is in μm, the parameter m is typically in the range 0.6 to 0.8 for water pressure from 0.1 to 50 MPa [14].

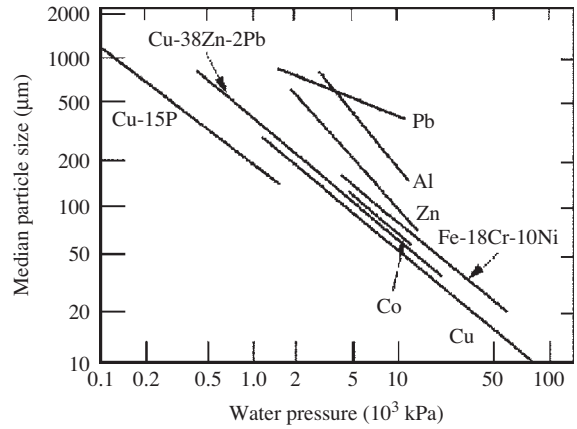

Figure 5.10 Particle size of water atomized metals as function of water atomized pressure.

Values of K are almost one order of magnitude higher for aluminum and zinc than for copper. In practice, this means that for two alloys water atomized under identical operating conditions, δ_m can vary by a factor of about 6. The K value evidently depends strongly on the physical and chemical properties of the molten alloy, in particular, viscosity and surface tension. Modification of the surface tension by the atmosphere (steam) to allow the formation of oxides is also expected to be important in terms of disintegration of the molten metal stream.

Increasing the melt superheat reduces δ_m in water atomization, primarily through the effect of temperature on viscosity and surface tension. For example, for zinc, an increase in superheat from 100 to 300°C reduces δ_m from 150 to 100 μm [13]. Similarly, in a cobalt-base alloy, increasing the superheat by about 150°C leads to decrease in δ_m of about 13.5% [15]. In addition to its effect on particle size, superheat is used as an operating variable to prevent freezing of the alloy in the exit nozzle of the tundish; simultaneously, the superheating leads to increase of melt flow rate through the tundish orifice, due to a decrease in melt viscosity.

The apex angle also influences particle size. With the apex angle increasing, the velocity component normal to the metal stream increases. It is shown [12,16] that δ_m decreases with increasing angle between the axis of the water jet nozzle and the liquid stream. Grandzol and Tallmadge represent this dependence in the form:

$$\delta_m = \frac{1}{v_w \sin\alpha} \quad (4)$$

However, there is a practical limit to the magnitude of the apex angle. Above about 50 degrees, flow

of the molten metal from the orifice of the tundish is impeded by the upward thrust of water, and the incidence of metal freeze-up at higher axis angles, especially at higher pressures (Figure 5.11). To decrease attenuation in water pressure, a short water-jet length is preferred, but again there are practical limits. It is normally found that using the apex angle to control fineness leads to dangerously unstable conditions. It is better to select a good stable setup with essentially zero rejection of melt and spray toward the jets and tundish and then provide the necessary pressure to achieve the desired particle size.

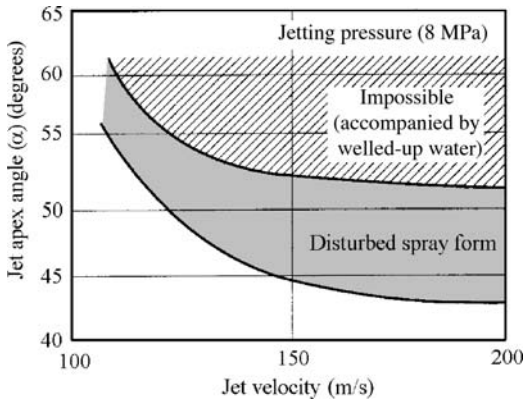

Figure 5.11 Effect of jet apex angle on stability of water atomization at various water velocities. (Source: Ref 16)

Powder Characteristics

Particles of water-atomized powder have generally an irregular shape with a pronounced uneven surface compared to gas atomized powders. For high-yield, low-cost production, and safe engineering, water atomization is usually preferred over gas atomization, providing powder characteristics are compatible with the application.

Particle Size Distribution

Generally, water-atomized powders exhibit log normal size distribution. Typical data for a range of metals and alloys and for differing operating conditions in water atomization are shown in Figure 5.12. Deviations from linearity using log normal-probability coordinates usually indicate operational instability, sampling errors or loss of fines. Minimum values of standard deviations (σ) are normally in the range 1.8 to 2.3, with some alloys on the low end of this range, e.g. Ni–B–Si and Fe–Si, while, for aluminum alloys

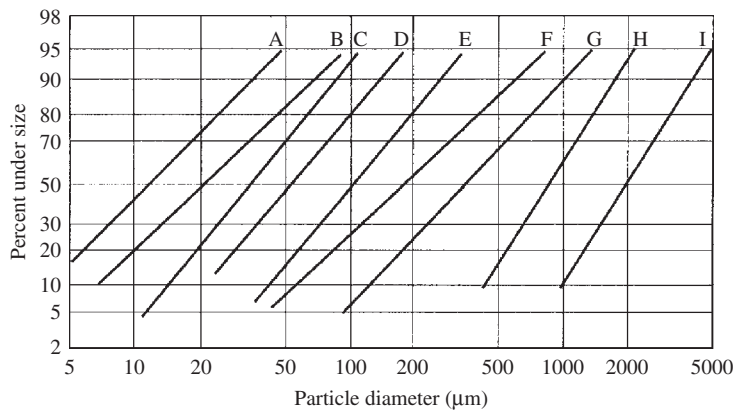

Figure 5.12 Typical water atomized particle mass size distribution. (Source: Ref 12)

	Alloy and water pressure	δ_{50}	σ
A	Copper atomized at 54 MPa	12	2.40
B	18Cr-10Ni-2.5Mo stainless steel atomized at 5 MPa	20	2.40
C	Fe-15Si atomized at 20 MPa	40	1.70
D	M2 high-speed steel atomized at 140 MPa	55	2.11
E	Fe-45Si for welding electrodes atomized at 4 MPa	100	1.70
F	Zinc for alkaline manganese batteries atomized at 5.5 MPa	180	2.34
G	Copper shot atomized at 2.0 MPa	400	2.30
H	15% phosphor copper shoot atomized at 0.15	800	1.76
I	15% phosphor copper shoot atomized at 0.05	2000	1.75

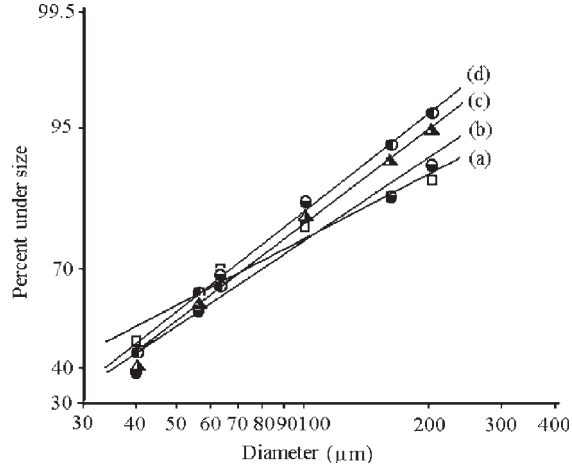

Figure 5.13 Typical particle mass size distribution of water atomized aluminum alloys:

Alloy and water pressure		δ_{50}	σ
(a)	$Al_{94}Fe_{2.0}Cr_{2.0}Ti_{2.0}$ alloy atomized at 15 MPa	40.5	2.96
(b)	$Al_{94}Fe_{2.5}Cr_{2.5}Ti_{0.7}Zr_{0.3}$ alloy atomized at 15 MPa	46	2.83
(c)	$Al_{94}Fe_{4.1}Cr_{1.3}Zr_{0.6}$ alloy atomized at 15 MPa	43	2.51
(d)	$Al_{94}Fe_{4.1}Cr_{1.3}Ti_{0.47}Zr_{0.13}$ alloy atomized at 15 MPa	42	2.5

(Figure 5.13) and the alloys which contain aluminum and chromium which form refractory oxides, values of σ are typically higher, namely 2.0 to 3.0. The standard deviation is calculated by:

$$\sigma = \frac{\delta_{84.1}}{\delta_{50}} = \frac{\delta_{50}}{\delta_{15.9}} \qquad (5)$$

where δ_{50}, $\delta_{84.1}$, and $\delta_{15.9}$, correspond to the particle sizes at the 50%, 84.1%, 15.9% cumulative weight percent levels, respectively.

Thus, the main influence on standard deviation, once a good and stable atomizing jet set-up is ensured, appears to be melt chemistry.

As a general characteristic of water atomization, δ_m and σ are not particularly sensitive to metal flow rate or the ratio of water flow to metal flow rate.

Figures 5.14 and 5.15 [17] illustrate the effects of melt nozzle diameter and pouring temperature for water-atomized copper powders on standard deviation and mass median diameter. The large effect of the atmosphere is observed (Figure 5.14). In fact, it is confirmed [3] that if copper is atomized with a large dissolved oxygen content, the powder is much finer. Thus, the large difference between nitrogen and air atmosphere may be due to this effect. Similarly, the chemistry may be directly influencing the standard deviation. The generally lower values of standard deviation at lower metal flow rates reflect

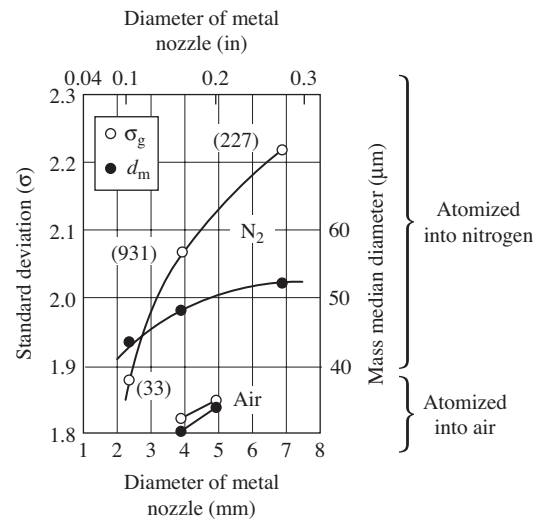

Figure 5.14 Effect of metal stream diameter on standard deviation of particle mass size distribution of water atomized copper powder. Pouring temperature 1200°C; figures in parenthesis show average metal flow in g/s. (Source: Ref 18)

the importance of collisions in broadening the size distributions.

It is appropriate to mention here that each commercial water atomization unit has its own feature operating characteristics. However, well-established proprietary empirical relations give a high degree

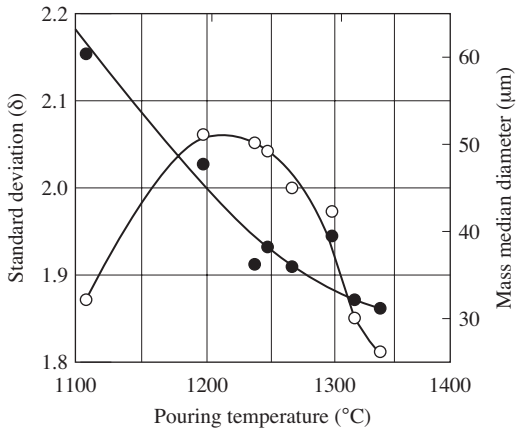

Figure 5.15 Effect of pouring temperature on distribution of water atomized copper powder. Metal stream diameter 4 mm; water flow 320 l/minute; water pressure 13.2 MPa; atmosphere nitrogen. (Source: 13)

of predictability in terms of operating conditions and powder properties, in particular, particle size. In addition to the aforesaid empirical formulas, there are others in the published literature that have been annotated by Beddov [19].

Particle Shape

The shape of water-atomized powder particles can vary appreciably. Most water-atomized powders are somewhat irregular in shape. Certain alloys can be produced with spherical or near-spherical shape, exhibiting apparent densities about 50% of theoretical, while others can be sponge like and extremely irregular in shape, in which case apparent densities are as low as 10–15% of theoretical.

During melt atomization, the irregular liquid metal drops under action of the surface tension forces tend to a spherical shape, the surface of which is minimal for a certain volume that corresponds to minimum free energy. At that, a particle shape is defined by relation of drop residence time in liquid state to spheroidizing time. Calculated values of the time necessary for solidification and spheroidizing of copper melt drops of different sizes [19] are shown in Figure 5.16. The heat-transfer coefficient dependence on water pressure, melt temperature and droplet size was taken into account. If the droplets' solidification time to spheroidizing time ratio value is equal to one or less, the solidified droplets will have an irregular shape.

In water atomization, the estimated spheroidization time for a 100 μm diameter droplet is in the range from 0.1 to 10 μs, depending on the magnitude of surface tension forces [12]. Freezing (solidification)

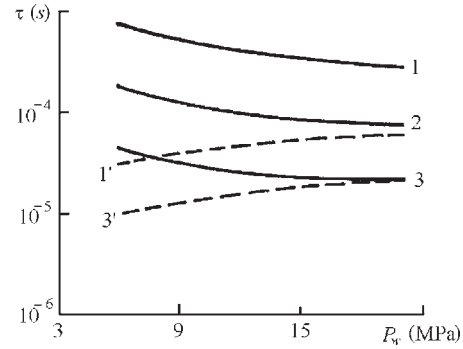

Figure 5.16 Solidification and spheroidizing times of copper melt droplets by pouring temperature 1140°C: 1–3 are cooling time curves; 1′and 3′ are spheroidizing time curves; droplet sizes in 640 μm diameter (1 and 1′), in 255 μm (2) and 102°μm (3 and 3′), accordingly. (Source: Ref 20)

times are of the order of 50–750 μs for elevated temperature aluminum alloys by pouring melt temperature 1250–1300°C (details of the analysis of droplet cooling rate are given in Chapter 13). Thus, solidification times are near to or shorter than spheroidization times, which are two or three orders of magnitude shorter than freezing times, and water-atomized particles are therefore predicted to be predominantly spheroidal in shape.

The formation of an oxide film on the surface of the droplet before it is in free fall and able to spheroidize can drastically affect particle shape. Elements that form refractory oxides prevent spheroidization by producing an oxide film with sufficient strength to oppose the forces of surface tension.

Thus, in terms of particle shape, droplets with very short freezing times tend to be more irregular and, in turn, are associated with low apparent densities. Accordingly, the longer freezing times characteristic of high melting point elements or alloys result in a more spherical particle shape.

Surface Morphology and Internal Structure

Water-atomized powders, along with their irregular shape, typically show a rough surface morphology and honeycomb. This characteristic is illustrated in water-atomized Al-6.0Zn-0.3 Mg-0.3Zr-0.5 Mn high-strength alloy (Figure 5.17) and Al-5.0Fe-5.0Cr-2.0Ti-1.0Zr elevated temperature alloy (Figure 5.18). The combination of irregular shape, surface roughness and porosity is an important feature of water-atomized powders, since green strength is enhanced by the mechanical interpenetration of irregular powders during die pressing.

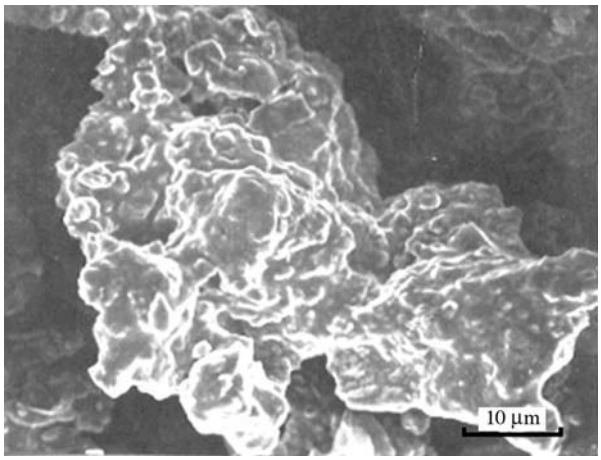

Figure 5.17 SEM micrograph of water-atomized powder of Al-6.0Zn-0.3Mg-0.3Zr-0.5Mn high strength alloy.

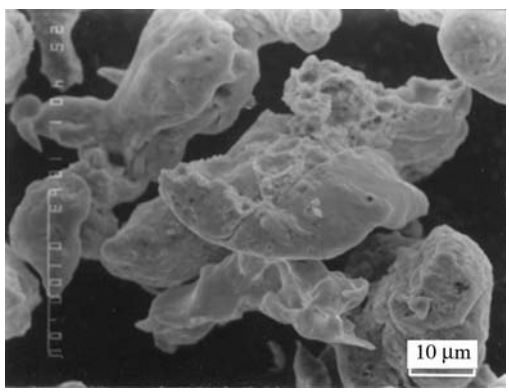

Figure 5.18 SEM micrograph of water-atomized powder of Al-5.0Fe-5.0Cr-2.0Ti-1.0Zr elevated temperature alloy. Superheat 200°C; diameter of gravity melt stream 7.0 mm.

Individual particles, or even different grains within a powder particle, differ in microstructure (Figure 5.19(a)). This is caused by differences in solidification behaviors of the solidifying fronts growing into the melt and of primary intermetallic phases distributed in the melt. Most of the particles exhibit a cellular or non-dendritic-like structure with an arm spacing of a few hundred nanometers in colonies a few microns in diameter (Figure 5.19(b)). Some other grains show a coarser background network structure where coarse primary intermetallics act as separate growth centers.

In addition to a non-dendritic structure, some other areas of individual particles show a subdendritic and cellular structure. Such observations can be explained by a significant intensification of the nucleation during crystallization by deep super cooling of the melt. The non-dendritic and subdendritic cell sizes are different for different particles. For example, the calculated cell size values shown in Figure 5.19(b) range from 1.2 to 0.94 µm that, in accordance with Eqn (1) in Chapter 13, correspond to cooling rates from 0.83 to 1.7°C/µs.

Powder Purity

Deoxidation of the melt plays an important role in the atomization process. The oxygen content of water-atomized powder is a function of the free energy of the reaction of the metal with water vapor and also of the reaction kinetics. For many water-atomized powders, oxygen levels are in the range 1000–4000 ppm by weight. The importance of the kinetic effect is exemplified by the appropriate oxygen levels in aluminum or high silicon alloys. In these alloys, a protective oxide film arises on the particle surface which prevents or retards further oxidation.

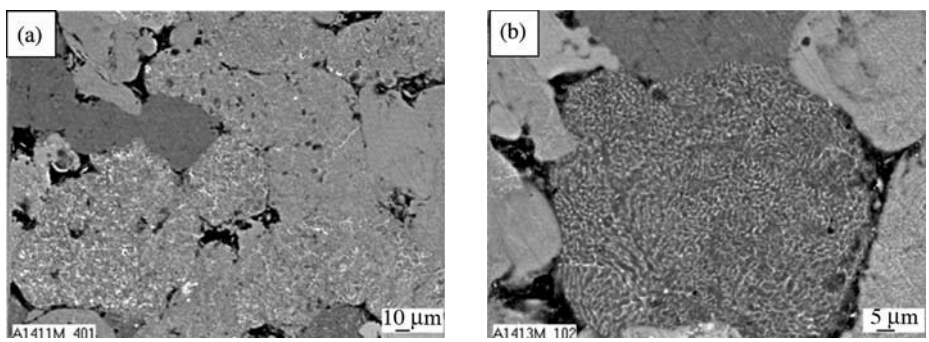

Figure 5.19 Microstructures of two typical metallographic sections of water-atomized powder particles of Al-Fe-Ce alloy in backscattering electrons with lower (a) and higher (b) magnifications.

Table 5.2 Characteristic properties of water-atomized powders

Metal alloys	Mass median particle size (δ_m) (μm)	Standard deviation σ_g	Apparent density (g/mL)	Oxygen content (ppm)
Ag	37	2.16	3.76	...
Ag-28Cu	32	2.3	3.37	285
Ag-25Sn-5Cu-1Zn	35	2.40	5.11	260
Al-3.92Fe-3.65Cr-3.3 Ti*	40.5	2.96	1.07	1200
Au	130	2.69	7.82	...
Au-20Ni	62	2.9	...	57
Bi	79	3.33	3.58	...
Cd	185	2.00	1.29	...
Cu	46	2.30	3.48	350
Cu	90	2.40	5.07	397
Cu-0.3Mg	31	2.51	2.01	1105
Ni	100	2.10	4.50	645
Ni-5Al	34	2.29	2.85	710
Ni-Cr-B-Si	51	1.69	4.26	...
Pt-10Rb	250	2.80	12.3	...
Sn	160	2.19	1.48	314
Sn	90	2.19	1.23	620
Zn	58	2.05	1.82	...

Source: Ref 12 and *IPMS data

The surface oxide of water-atomized powders is non-uniform in thickness. So, with water-atomized powders, three-dimensional film islets with a typical thickness of 30–40 monolayers usually cover 30–70% of the particle surface. The rest is covered by a thin oxide film about 3 to maximum 8 monolayers [21]. Table 5.2 gives the characteristic properties of water-atomized powders, including oxygen content.

The increase of oxygen content can be accommodated by modifying the atomization conditions. For example, the use of inhibitors in combination with the control of hydrogen ion level, and suspension temperature, during the atomization process can lead to a decrease in the oxygen content to the level of gas-atomized powders [22]. The Au-Ni brazing alloys normally have an oxygen contain about 200 ppm. By using inert purging gases in the melting process, the oxygen level is reduced to 150 ppm. Further reductions in oxygen level to 100 ppm and 40–50 ppm can be achieved by deionized water or by the addition of alcohol to the water. The use of anti-foaming agents in the atomizing water can further reduce oxidation and increase the cooling rate [15].

Oil Atomization

The oil-atomization process should avoid the problem of powder oxidation. In the early 1980s, Simetomo Metals developed the oil atomization process for the commercial production of relatively high carbon (0.4 wt%) steel [15]. Oil-atomized powders resembled water-atomized powder in particle size. Their densities are intermediate between water- and gas-atomized powders as the cooling rate is slower and oxidation much less. However, carbon pickup occurs to an extent depending on metal temperature and carbide-forming tendency of the melt [23].

Gas Atomization

Gas atomization (GA) is the process in which the liquid metal is dispersed by a high-velocity jet of air, nitrogen, argon or helium. Gas atomization is used for the commercial production of powders of copper, copper alloys, aluminum and its alloys, magnesium, zinc, titanium, titanium alloys, nickel-base alloys, cobalt-base alloys, lead, tin, solder, precious metals, refractory metals, beryllium, etc.

Air atomization of aluminum, copper, brass and zinc powder accounts for about 250 000 tonnes. Inert gases are used when the oxygen content must be kept low, or when atomizing reactive metals such as the superalloys and titanium. The worldwide annual tonnage of inert gas atomized metal powders is much less than for water-atomized powders. The relationship between the shipments of ferrous and non-ferrous

powders is about 4 to 1. But, in market value terms, aluminum, silver and zinc are all close to the value of iron powders [1, 24]. The price in $/kg of metal powders produced, their volume in t/year, and their total market values in $billions are shown in the Introduction in this book.

Gas atomization differs from water atomization in many aspects. Rather than being dominated by the pressure of the medium like water atomization, it is found that the gas-to-metal ratio is the dominant factor in controlling particle size. A feature of GA is the fact that an increase of pressure above 0.1 MPa, at which the sonic velocity is reached, gives only small increments in gas velocity. In contrast, to reach sonic velocity (in air or nitrogen) with a water jet, a pressure of nearly 40 MPa is needed and the velocity increases according to the square root of the pressure. Moreover, gas atomization takes place by the action of a continuum on another, while in water atomization a stream of droplets in an entrained gas flow acts on a continuum. The density of the water medium is about a thousand times higher than the gases used, giving much greater impact.

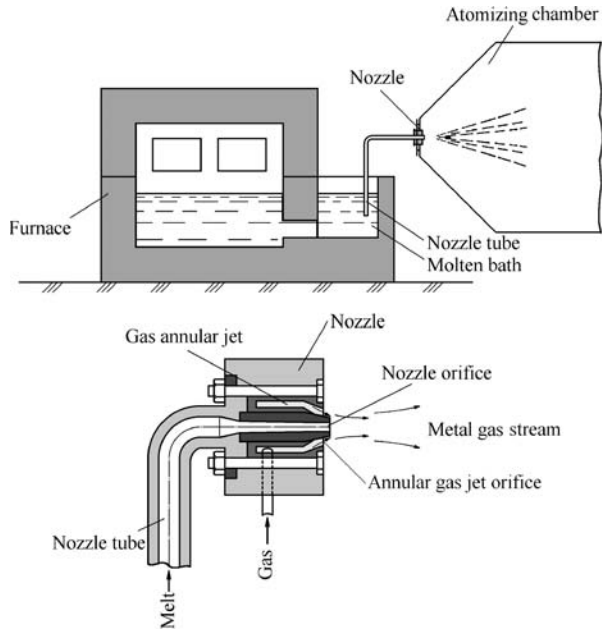

Figure 5.20 VAMI aspirating nozzle design with horizontally molten metal stream.

Gas Atomizing Units

Gas atomizing units also come in a much wider range of designs than water atomizers. The earliest gas atomization was with steam, patented in 1872 by Marriott of Huddersfield. The very simplest design of atomizer is to let a metal stream to fall onto a horizontal gas jet and this has been used for zinc powder production. The earliest scientific worker in this field seems to have been Professor Hall, founder of the Metals Disintegrating Co. His patent in the late 1920s [25] represents a kind of close-coupled atomizer for aluminum atom-ization. The basic design shown in this patent is still in use and has yet to be improved in any radical manner. A similar unit developed by VAMI is shown in Figure 5.20. The atomizing gas is delivered through an annular orifice around the nozzle at the converging angle. The gas flow creates the suction (aspiration) effect at the tip of the nozzle that draws the molten metal into the nozzle. The amount of gas delivered by the nozzle is controlled by the size of the air gap and pressure and temperature of the gas. Rate of metal flow and resultant powder particle size are influenced by the aspirating force, the nozzle metal orifice diameter and the vertical distance between the nozzle and molten metal level.

This atomizer design aims to contact the liquid metal stream with the gas at or close to the gas jet exit plane where the highest jet velocities exist. It leads to efficient break-up of the liquid, resulting in finer powders and is the preferred method for aluminum and other low-melting-point metals. It can be operated vertically upwards or down wards or in the horizontal position. Careful design of the atomizer is required, however, to avoid freezing of the metal by the gas jet, which can lead to solidification at the nozzle tip.

Many gas atomizer designs are known. They are classified as 'free fall', 'confined' or closed nozzles (Figure 5.21(a)) and 'internal mixing'. The closed nozzle designs are also as known as close-coupled nozzle designs.

For free gas atomization (Figure 5.21a), the key process variables are similar to those of water atomization (see Figure 5.3). In this atomizer, the liquid metal issues in the form of a stream from a tundish and falls 100–200 mm by gravity. Then it is atomized either by means of discrete or an annular directed at the point of meeting with the metal stream. This method is easy to operate but inefficient and is not suitable for making fine powders.

In the 'internal mixing prefilming' atomizer type, the gas and liquid metal are mixed together before expanding into the atomizing chamber [26].

Confined Nozzle Designs

This nozzle design (see Figure 5.21(b)) makes it possible to increase the yield of median particle size powder

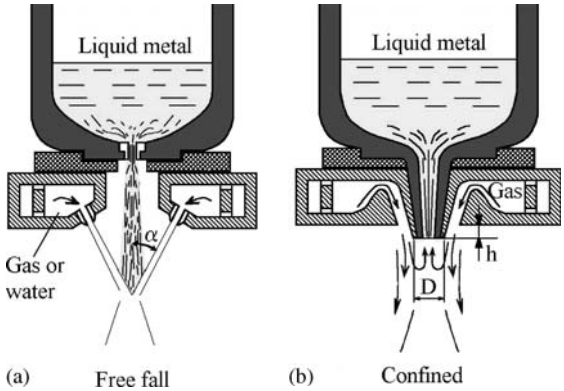

Figure 5.21 Atomizer designs of two types: (a), free fall design (gas or water) and (b) confined nozzle design (only gas). Design characteristics: α, angle formed by free-falling molten metal and atomizing medium jet; D, diameter of confined molten metal nozzle end; h, protrusion length of melt nozzle.

(40–60 μm) by maximizing the gas velocity and density at the meeting with the metal stream [16]. However, the use of these units can cause the freezing of the molten metal at the end of the tundish nozzle, which immediately stops the atomizing. Along with this, the interaction of the gas stream with the nozzle tip can form either under pressure or positive pressure, varying from an underpressure that can significantly increase melt flow rate to an inverse pressure sufficient to stop it and blow gas into the tundish. Thus, great care is needed in setting up closed nozzles and control during atomization.

The WIDEFLOW gas atomizer based on the confined nozzle principle is illustrated in linear modification (Figure 5.22) [27]. This atomizer involves two chambers, a high-pressure chamber (autoclave), containing melting and pouring units, and a low pressure atomization chamber divided by a linear Laval gas nozzle. The pressure difference between the two chambers forces the gas accelerated flow through the converging linear Laval nozzle to sonic velocity, when the pressure ratio exceeds the critical value. Kinetic energy of ultrahigh velocity gas flow is transferred efficiently to the atomization of thin melt film. Using nitrogen or argon, mean particle diameters about 10 μm can be achieved with pressures of 2.0–2.5 MPa [28].

Ultrasonic Gas Atomization

Confined atomizers are of two types: conventional (see Figure 5.21(b)) and ultrasonic (Figure 5.23). The ultrasonic designs use the Hartman tube principle to apply high-frequency pulsation to the gas stream, with gas exit velocities reported to be Mach

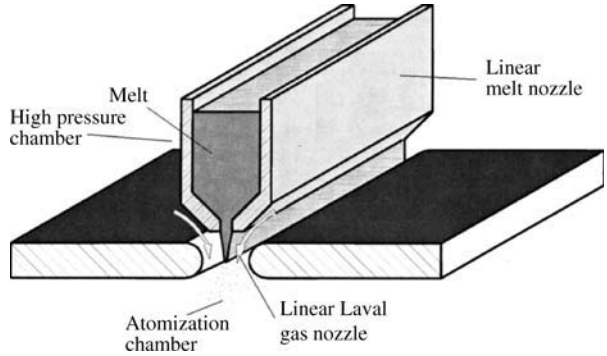

Figure 5.22 Simplified drawing of the WIDEFL0W confined linear nozzle design.

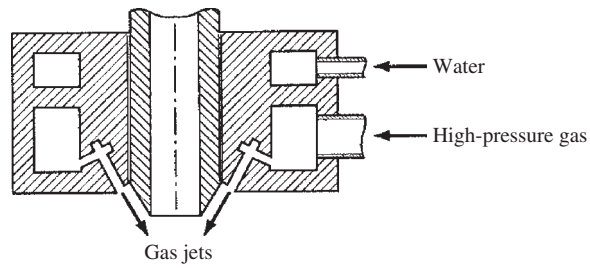

Figure 5.23 Ultrasonic gas atomizer. (Source: US Patent 2,997,245, Aug 1961)

2 to 2.5 and the major pulsation frequency at about 100 000 Hz. HEVs ultrasonic atomization unit includes an induction melting unit, atomizer, transducer, transfer tube and tubular resonator [29]. Classification of the pneumo-acoustic atomizers, development of new devices and procedures for ultrasonic gas atomization are given in [30].

Prefilming Nozzle Design

In several confined designs, the circulation created by the gas flowing up the side of the tundish nozzle causes, due to aspiration force action, the molten metal to spread across the face of the ceramic nozzle to its edge, where it is sheared by the flowing gas [31]. These nozzle designs are referred to as 'prefilming' (Figure 5.24(a)) and are quite widely used.

The regime when a thin film is formed on the melt nozzle top is the preferred operating regime for producing fine powders. When the metal flow rate is too high, the filming effect is partially lost and some of the metal is entrained into the low-velocity wake and does not film effectively [32]. Such a regime leads to coarser powders and to the formation of undesirable flakes in the powder.

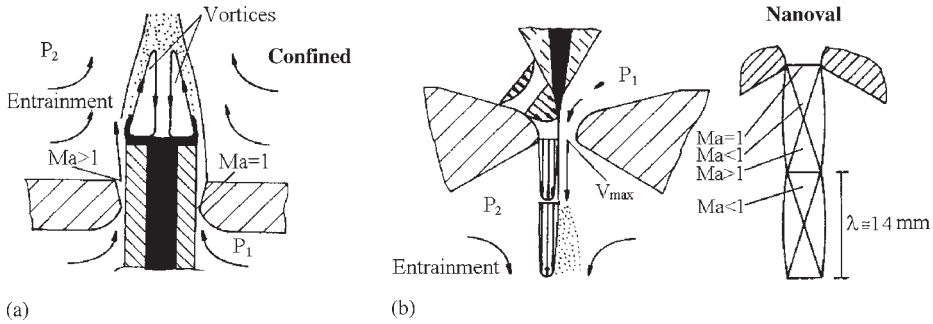

Figure 5.24 Schematic of prefilming nozzle design (a) and Nanoval design (b).

The low pressure (suction, aspiration) created at the nozzle tip is a useful feature of the prefilming nozzle design. It is employed to draw the liquid metal into the melt nozzle from the crucible in up-draught operation, as mentioned above. Additionally, the presence of suction at a point of contact between the gas and liquid avoids the potentially hazardous blowback effects observed in free fall nozzle designs for certain jet geometries.

At the same time, by the air atomization a sudden stoppage or decrease of its flow rate can lead to ignition or explosion of the suspended solid powder in case of active metals or alloys.

The level of suction created by a nozzle is found to be extremely sensitive to nozzle geometry, atomizing gas nature and operating gas pressure [32].

Nanoval Nozzle Design

In the Nanoval nozzle design [33], a metal melt stream is broken up by the action of friction forces between the atomization gas and the liquid (Figure 5.24(b)). Because the metal stream is always kept very thin and it is delivered directly to the throat of the nozzle, this design is capable of producing very fine powders. The comparison of mean particle sizes by Nanoval and conventional confined nozzle design is represented in the form of mass median diameter dependence on specific gas momentum, shown in Figure 5.25.

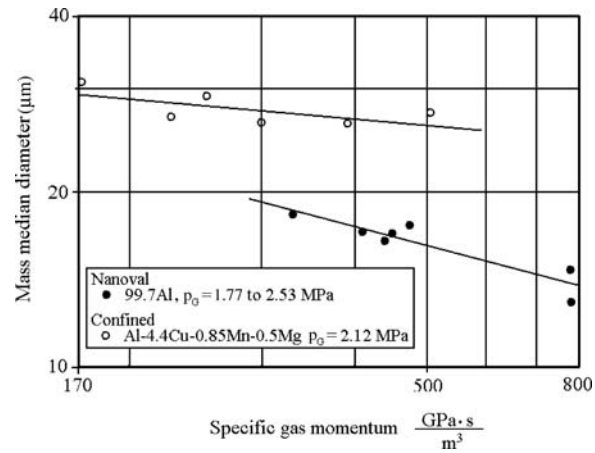

Figure 5.25 Comparison of mean particle sizes by Nanoval and conventional confined atomizing nozzle designs.

Pressure-swirl Hybrid Prefilming Atomizer

This atomizer combines pressure-swirl atomization and ring-gas atomization. In the first stage, a film is generated followed by gas jet atomization in the second step [34]. The pressure-swirl-metal chamber, atomization chamber and gas-recirculation system are the main components of the powder atomization unit. Figure 5.26 [35] shows schematically a pressure-swirl atomizer. Due to overpressure, the molten metal flows tangentially into the swirl chamber, leaves it through a small cylindrical hole (D_L) and forms a

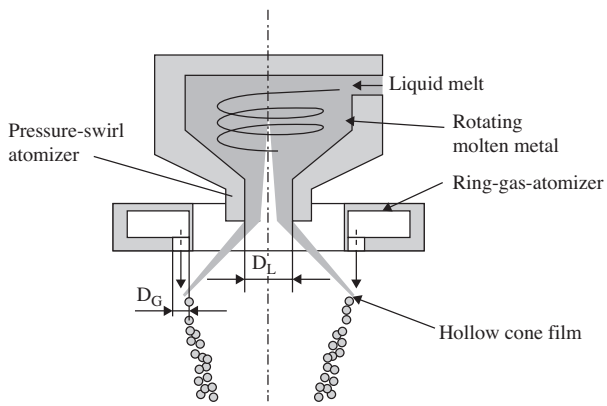

Figure 5.26 Pressure-swirl hybrid prefilming atomizer.

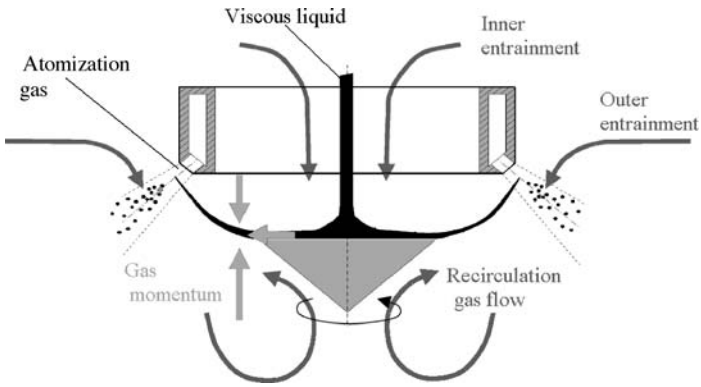

Figure 5.27 Prefilming hybrid atomizer for viscous melt atomization. (Source: Ref 36)

swivelling hollow cone film of molten metal. The film is subsequently atomized by the gas jets through the orifices (D_G).

Spherical tin powders with median diameter 10–20 μm and standard deviation below 2 were obtained by superheat 100°C, gas (nitrogen) pressure 1.0 MPa, gas to metal ratio 1.3, and with a melt flow rate between 160 and 190 kg/h.

Prefilming Hybrid Atomizer

This has been developed for viscous melt atomization [36]. Viscous melts, such as oxidized metals or slags, have a comparably high viscosity. The prefilming hybrid atomizer is shown in Figure 5.27. Their local flow regimes are distinguished by the difference from where the ambient gas interacts with the atomization gas. The inner entrainment reaches the atomization area through the atomizer liquid stream passage. The outer entrainment reaches the atomization area directly and the recirculation gas flow reaches the atomization area from below the rotary disk. The aim of the prefilming hybrid design is to generate a maximum recirculation momentum so that the film is transported closer to the external mixing atomizer gas outlet.

Process Parameters

In conventional gas-atomization processes, the atomization pressures are typically in the range 0.5 to 4 MPa and gas velocities in the nozzles range from Mach 1 to 3. However, in free-fall atomizers, gas velocities in the impingement zone usually have fallen to 50–150 m/s (for air or nitrogen). Typically, gas-atomized powders are usually spherical with log normal size distribution. Average particle sizes are usually in the range 10 to 300 μm with a standard deviation of about 2; oxygen content is the range of 100 to 1000 ppm. Prealloyed alloys are made commonly by inert gas atomization. Worldwide annual tonnage of inert gas-atomized powder is much less than that of water-atomized powders, probably amounting to more than 50 000 tonnes per year. Metal feed rates are lower than in water atomization and melt batch is smaller. However, total tonnage of air-atomized powders, especially zinc and aluminum, as well as copper, tin, lead and copper alloys, probably exceeds 400 000 tonnes per year [1]. Air atomizers operate continuously for many hours or round-the-clock. Multinozzle units are often used to boost yield on aluminum and zinc.

In conventional inert gas or air atomization, typical metal flow rates through single-orifice nozzles are in the range 1–90 kg/min. Capability of plants varies from very little laboratory units to immense plant such as ANVAL Atomizer 1 (Figure 5.28), which is the biggest inert-gas atomizer and is designed for producing large tonnages of superalloy and other alloy powders. Melting takes place in two 5.5-tonne induction furnaces. A plasma-heated tundish is used. Due to the height of the tower, powder with up to 1 mm particle size can de produced. Very fine powder can also be produced for applications such as MIM.

In conventional atomizers, typical gas flow rate ranges from 1 to 50 m^3/min at a pressure range of 350 kPa to 4 MPa. The superheat of molten metal (the temperature differential between the melting point and the temperature at which the molten metal is atomized) is generally about 75–150°C. In gas atomization with inert gas, the cost of gas consumption is significant, and a means of circulation to promote gas reuse is desirable, especially in large-scale facilities.

In practice, for a given gas nozzle design and size, mean particle size is controlled by the pressure of the atomizing medium and the melt flow rate, which is regulated by nozzle diameter and nozzle suction. For all nozzles, the velocity of the gas usually 'chokes' at sonic velocity (about 300 m/s for nitrogen and argon) in the narrowest region of the nozzle.

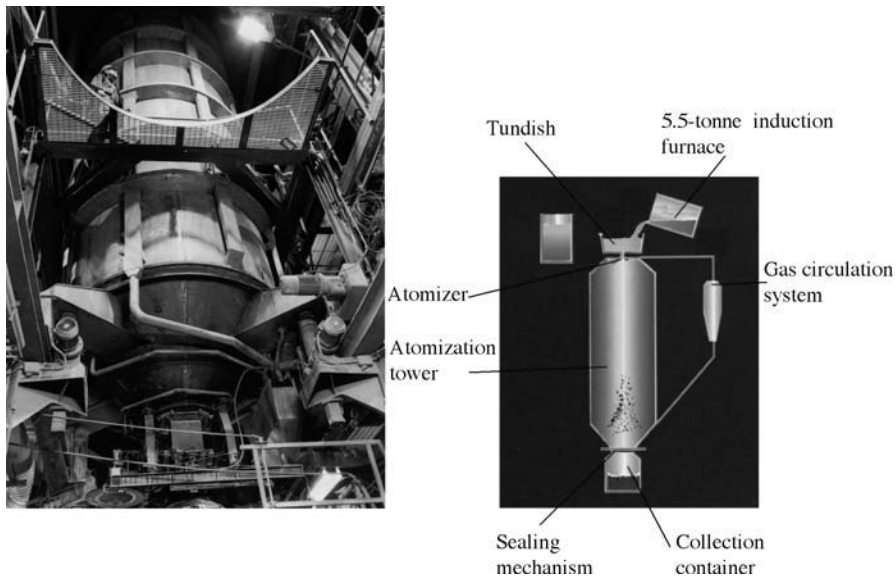

Figure 5.28 ANVAL Atomizer 1. Courtesy of ANVAL.

Therefore, the amount of gas flow (Q) depends on gas pressure, temperature and nozzle area. For ideal conditions and zero velocity on the entrance side of the nozzle, gas flow can be expressed [3]:

$$Q = \omega\left(\frac{2}{k+1}\right)^{\frac{k+1}{2(k-1)}} g\frac{p\sqrt{2g}}{\sqrt{RT}} \tag{6}$$

where ω is the cross-section of gas nozzle at exit; k equals C_p/C_v, the ratio of specific heat at constant pressure and volume, correspondingly; p is the gas pressure in reservoir; T is the temperature in gas reservoir; R is the gas constant; and g is the acceleration due to gravity. For nitrogen $k = 1.4$.

As a compressible fluid passes through a nozzle, a drop in pressure and a simultaneous increase in velocity result. If the pressure drops sufficiently, a point is reached where, in order to accommodate the increased volume due to expansion, the nozzle design must diverge. Thus, nozzles for supersonic velocities must converge to a minimum section and diverge again.

A comparison on the basis of how much powder surface is generated per unit of atomization gas spent can be used for evaluation the gas efficiency. This criterion accounts for higher gas consumption requirements when higher gas pressures are applied to produce finer powders. Confined nozzle designs in comparison with consumption ones give higher efficiencies at a comparable gas to metal ratio [37]. A simple equation of median particle size dependence on gas/metal ratios can be used:

$$\delta_m = \frac{k}{\sqrt{G/M}} \tag{7}$$

where k is a constant for the process and G/M is the gas/metal ratio, which is variously measured in kg/kg or cubic meters of gas per metal mass (m^3/kg). Source [16] involves typical values of k for confined nozzle designs.

Models of Gas Atomization

Superheated metal melts may be considered as Newtonian liquids; in this connection their interaction with the gas jet is expressed by criterial dependences. The most empirical formulations for definition of an average particle size in real atomization systems use the aerodynamic Weber number:

$$We_g = \frac{\rho_g v_g^2 d_0}{\sigma_m} \tag{8}$$

This criterion represents the balance of the break-up force, related to gas kinetic energy through the gas density, ρ_g, and v_g^2, that is resisted by melt surface tension, σ_m, acting over a specific melt stream diameter, d_0.

Generally, in each model of droplet formation, a stability criterion involves the Weber number of the liquid metal. The first attempt to develop a model

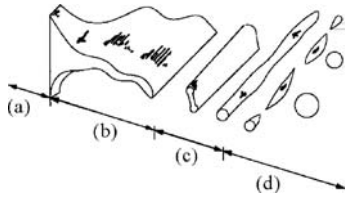

Figure 5.29 Model for the disintegration of a liquid sheet by a high velocity jet of gas: (a) stable sheet; (b) growth of waves in sheet; (c) ligament formation; (d) ligament breakdown.

of the three steps droplet formation process seems to have been made by Dombrovski and Johns [38]. Proposed mechanisms of droplet formation involve:

- the initiation of a sinuous wave which rapidly increases in amplitude
- detachment of the wave from the layer of the liquid to became a ligament whose dimensions depend on the wave length λ at disintegration on wave number k_w (i.e. $2\pi/k_w$)
- breakdown of ligaments into droplets (Figure 5.29).

In Bradley's mathematical model, known as the capillary wave model [39,40], the liquid is considered to be a horizontal infinitely deep phase, initially not moving, being swept by a compressible gas phase with a uniform velocity parallel to the liquid surface. Rayleigh instability was invoked for the break-up of the ligament into spherical drops. In the first stage of the atomization process, the critical wave number k_{max} with the fastest growing amplitude is determined from quadratic equation in k and includes a dependence on the kinematic viscosity of the liquid, the densities of the gas and liquid phases, the liquid/gas interfacial energy that opposes the growth of the wave, and the Mach number M of the atomizing gas.

In the second stage of atomization, Bradley suggested that the ligament diameter D is related to the wavelength λ_{max}, i.e. $2\pi/k_{max}$ by linear dependence:

$$D = \varepsilon\lambda_{max} = \frac{2\pi\varepsilon}{k_{max}} \tag{9}$$

where the parameter ε (of the order of 0.25) was defined in earlier studies on the air atomization of water.

The resultant droplet diameter δ is expressed:

$$\delta = \frac{2.95\sigma_m}{L\rho_g v_g^2} \tag{10}$$

where σ_m is the liquid surface tension (N/m), ρ_g is the density of the gas (kg/m^3), v_g is the sonic gas velocity (m/s), L is a dimensionless parameter, the function of the Mach number M and knowing the value of M during gas atomization; L can be defined by [41].

A comparison of the experimental data of See and Johnston to Bradley's predictions for the nitrogen atomization of lead sees that the model gives agreement approximately within a factor of two [42]. At its present design, Bradley's model does not give any indication of the origin of the spread in powder production by gas atomization.

The other often-cited models are the capillary and acceleration wave models of Ingebo [43]. Here, the Reynolds number is an important part of the Ingebo expressions for both capillary and acceleration wave break-up. The Reynolds number

$$Re_L = \frac{\rho_L (v_g - v_L)^2 d_0}{\mu_L} \tag{11}$$

contains the dimensionless balance of gas kinetic energy through $(v_g - v_L)^2$, as related to the dynamic viscosity, μ_L, in the melt with a density, ρ_L, in the melt stream diameter, d_0.

The resulting Ingebo equation is:

$$\frac{d_0}{\delta_m} = c_0 (We\ Re_L)^m \tag{12}$$

where c_0 and m are adjustable constants; for area $WeRe_L > 10^6$ $c_0 = 0.027$ and $m = 0.4$, then

$$\delta_m = 37 d_0 [We\ Re_L]^{-0.4}$$

A modified capillary wave model in melt atomization was applied in several works [44,45]. Ternovoy and colleagues [45] considered the atomization of free melt stream by annular gas jet with hollow cone of metal formation. The instability wavelength λ_f with the fastest-growing amplitude in the metal film was defined in accordance with [46]:

$$\lambda_f = \frac{1.5\gamma}{\rho_g v_g^2} \tag{13}$$

where γ is the specific surface energy of a melt, ρ_g is the gas density, v_g is the gas velocity at the exit of the melt nozzle.

The droplet formation is considered as break-up of the melt micro-jets by instability wavelength $\lambda_{\mu j}$ with the fastest growing amplitude in metal micro-jets and is described in accordance with [46] by the expression:

$$\lambda_{\mu j} \approx 4\pi \left(\frac{v_m^2 \rho_m \delta_{\mu j}^3}{8\gamma} \right)^{1/4} \tag{14}$$

where v_m is the kinematic viscosity of a melt, ρ_m is the melt density and $\delta_{\mu j}$ is the diameter of the micro-jet.

The resulting semi-empirical formula for the droplet diameter definition is:

$$\delta_m = \frac{1.88 v_m^{0.4} \rho_m^{0.2} d_m^{1.26}}{\gamma^{0.026} \rho_g^{0.17} R_{tr}^{0.63} v_g^{0.34}} \left(\frac{gh\rho_m + \Delta p}{gh\rho_m - 2\Delta p} \right) \left(\frac{G_m}{G_g} \right)^{0.3} \quad (15)$$

where d_m is the melt jet diameter at the exit of the melt nozzle, R_{tr} is the film opening radius in position of toroidal thickening on its periphery, g is the acceleration due to gravity, h is the melt height in the tundish, Δp is the pressure differential between furnace chamber and the exit of the melt nozzle, G_m melt mass flow, and G_g gas mass flow.

More recently, improved flow visualization techniques used to study melt atomization dynamics do not confirm the formation of film hollow cone in conditions of atomization of free melt stream by annular gas jet [47]. Through that, the authors [45] obtained the tolerable convergence of median particle size values calculated on the suggested formula with measures for argon or argon/helium mixture atomization on a confined nickel alloy jet.

The pressure-swirl atomization principle allows formation of the film metal hollow cone as is shown in Figure 5.26. Here, a conical film of melt created by a pressure swirl nozzle and shaped by centrifugal forces is atomized by high- velocity gas jets. The physical model of such combined atomization process was represented in work [48]. There are considered to be the following stages of the atomization process (Figure 5.30):

1. transmission of instability wave in a film across and along the velocity vector owing to oscillation processes caused by external and internal factors. The instability wavelength κ_f with the fastest-growing amplitude in a metal film was introduced in accordance with [46]. Depending on the physical properties of the liquid and gas, two schemes are suggested: with a thickening of a film in toroidal form in accordance with wavelength (Figure 5.30 (side a)) and when a film is just bending (Figure 5.30(side b))
2. formation of a liquid torus on peripherals of a film as a result of transmission of a longitudinal wave with the fastest growing amplitude

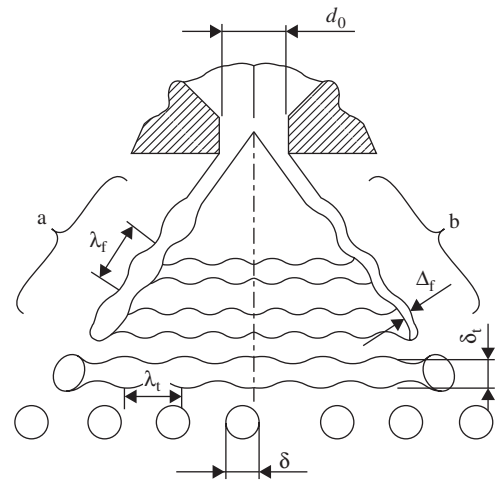

Figure 5.30 Model of the pressure-swirl atomization process: d_0 is the melt metal nozzle orifice diameter, Δ_f is film thickness in zone of impingement with secondary atomization gas jet, δ_t is the diameter of max torus cross-section in zone of impingement with secondary atomization gas jet, λ_f is the wavelength of film instability, λ_t is the wavelength of liquid torus and δ is the atomized particle diameter. (Source: Ref 48)

3. transmission of instability of toroidal peripheral area
4. all previous stages coincide with the above described model [45], while the final stage differs because it consists of secondary atomization of previously broken up film ligaments (torus or drops in dependence on atom-ization conditions) under the action of a high gas pressure jet.

The thin film represents a surface for efficient disintegration in order to achieve fine particle sizes and narrow size distribution using low specific gas consumption.

On the basis of this model, a formula for definition of particle diameter was suggested:

$$\delta = k\varphi^{0.46} \frac{v_m^{0.17} \rho_m^{0.08} \sigma^{0.38} d^{0.92}}{R_f^{0.46} \rho_g^{0.46} v_g^{0.92}} \quad (16)$$

where k is the coefficient of the nozzle geometry; φ is the unfilled coefficient for the melt nozzle orifice of d diameter; v_m is the kinematic viscosity of a melt; ρ_m is the density of a melt; σ is the surface tension of the melt; R_f is the radius of the film at the point of break-up; ρ_g and v_g are the density and velocity of a gas stimulating the film disturbance.

Table 5.3 Tin powder properties produced by means of the pressure-swirl atomization process

Oxygen contentin the atomization chamber (ppm)	Melt temperature (°C)	Melt pressure (MPa)	Melt flow rate (kg/h)	Gas pressure (MPa)	Gas flow rate (m^3/h)	Mass median diameter (μm)	Standard deviation (δ_{84}/δ_{50})
<100	290	0.7	180	0.7	109	33.5	1.85
100	290	0.7	180	0.7	109	22.8	1.6
300	290	0.7	180	0.7	109	22.1	1.6
500	290	0.7	180	0.7	109	24.6	1.6

The estimation of the mass median diameter offered by Eqn (16) shows sufficient comparability between calculated and experimental values for tin, tin–lead solder (61Sn–39Pb) and copper alloy (Cu–15Sn–5Pb–4Ni) in experiments by gas/metal ratio values in the range from 0.15 to 0.35 m^3/kg [48]. An effect of oxygen content on powder properties was revealed (Table 5.3).

Traditionally, gas atomization by means of close-coupled nozzles is believed to involve the formation of a melt film at the nozzle edge [49], as shown in Figure 5.31. Fine particles are thought to form as a result of the primary breakup of the melt film upon its interaction with supersonic gas flow at the nozzle edge. Further, even if low melt flow conditions that favor filming are used, it has been suggested that secondary breakup still plays an important role in determining particle size [50].

More recently, a microsecond-exposure spark schlieren technique allow us to visualize the melt atomization process along with the atomizing gas flow features, providing a look at the fluid dynamic interactions during atomization [47]. These experiments indicated more complex atomization behavior, including a primary breakup stage close to the nozzle tip, followed by a finer secondary breakup stage where the coarse droplets are disintegrated under high shear into fine powder. Therefore, several authors [50,51] have discussed the apparent dominance of secondary atomization and break-up mechanisms in most studies of close-coupled gas atomization. However, this model version does not exclude the importance of primary atomization to minimize the spread of $\Delta v | v_g - v_m |$ values.

The increased understanding of the atomization process discovers new ways to approach the problem of particle size control and atomization efficiency. In this connection, in close-coupled gas atomization, there is a considered description of the two gas flow situations that are termed open wake condition

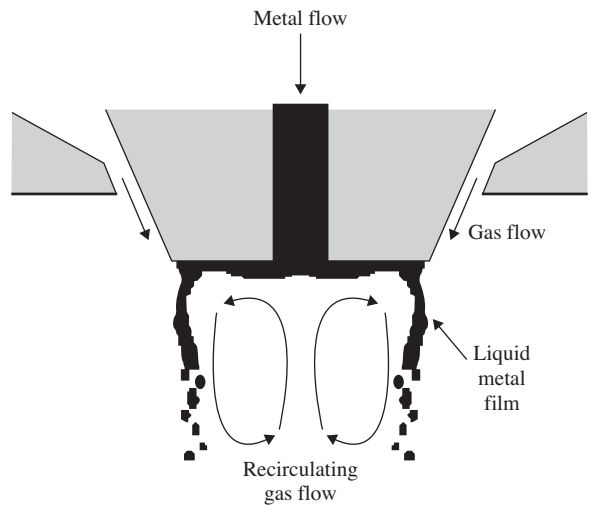

Figure 5.31 Metal filming view in gas atomization. (Source: Ref 49)

[51,52], as shown in Figure 5.32(a) and closed wake conditions in Figure 5.32(b), where the sketches are of a central cross-section and may apply to either a discrete jet nozzle ensemble or an annular slit nozzle with the same melt tube arrangement.

A more complicated gas flow situation has often been developed purposefully for the production of high yields of fine droplets where the shear wall gas flow is interrupted by a Mach shock disk. The Mach shock disk can appear during high pressure operation of either an annular slit [52] or discrete jet [53]. The wake closure effect and its associated Mach shock can present an additional kind of atomization energy coupling.

The pressure value on the liquid metal nozzle tip is an important parameter in close-coupled gas atomization. The pressure formation on the melt nozzle tip in dependence on gas pressure is shown in Figure 5.33.

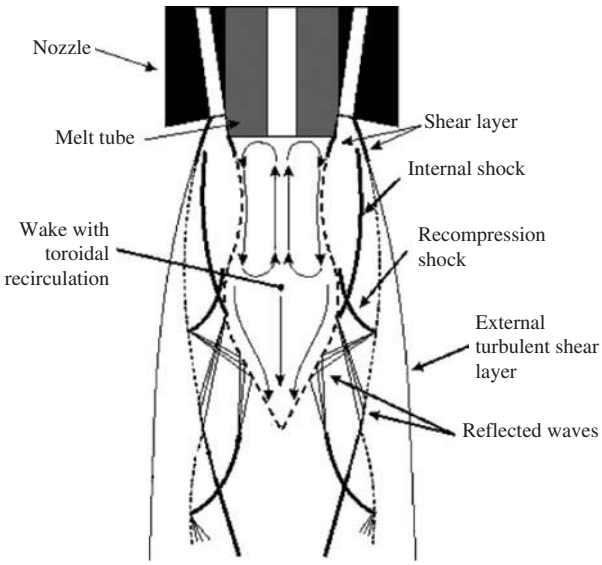

Figure 5.32 Schematic of (a) open wake and (b) closed wake gas flow patterns in close coupled gas atomization. (Source: Ref 53)

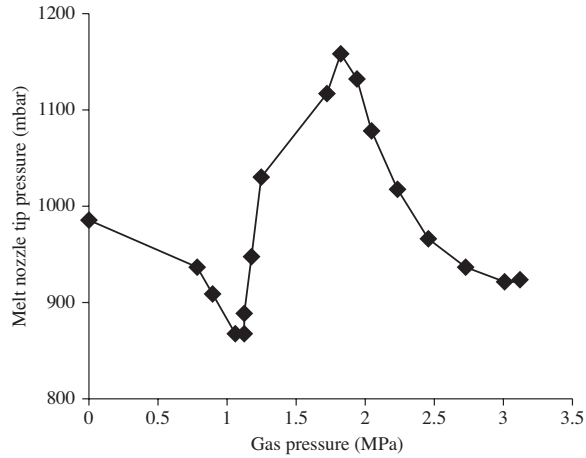

Figure 5.33 The pressure formation on the melt nozzle tip in dependence on gas pressure in close-coupled slotted nozzle design (by the constant protrusion length 10 mm).

Gas Atomized Powders

Particle Size, Size Distribution, Shape and Surface Morphology

There is a comprehensive literature base on gas atomization in terms of the effect of operating conditions on powder properties [14,15,56].

One of the most important single parameters controlling particle size in gas atomization is specific gas consumption. It can be expressed as a mass ratio of gas to metal flow or as the ratio of gas volume to metal mass. Data for several metals and alloys conform to an equation of the form:

$$\delta_m = KF^{-1/2} \tag{17}$$

where K is a constant and F is the specific gas consumption in m^3/kg. The value of K is a function of nozzle design and alloy properties [15].

Specific gas consumption is also an important process parameter in controlling δ_m in ultrasonic gas atomization [42,57]. For an aluminum alloy at a fixed atomizing gas pressure, median diameter value can be varied from $\approx 250\,\mu m$ to below $50\,\mu m$ when the mass flow ratio of gas to metal increases from 0.3 to 2.0. A decrease in δ_m is also predicted with increasing gas pressure.

Gas-atomized powders generally have a log normal size distribution, with standard deviation normally around 2.0 ± 0.3. The values of π generally decrease as δ_m decreases and most data show an in empirical relation of the form [56,58]:

$$\sigma = a\delta_m^b \tag{18}$$

where a and b are constants.

Lubanska [58], by comparing the literature on gas-atomized metal powders and by using a relationship

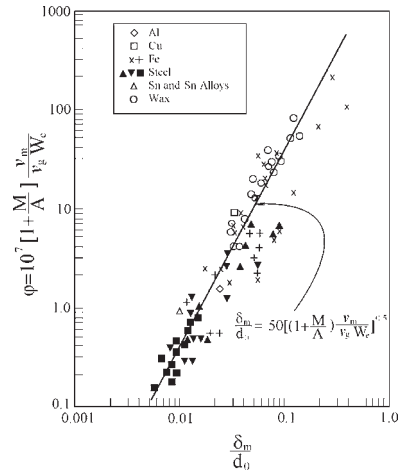

Figure 5.34 Lubanska correlation (Eqn 19) for air atomization.

developed by Wigg [59], derived an empirical equation for the average particle size (δ_m). In dimensionless form, Lubanska's formula is:

$$\frac{\delta_m}{d_0} = K\left[\frac{v_m}{v_g}\frac{1}{We}\left(1+\frac{M}{A}\right)\right]^{1/2} \tag{19}$$

where *We* is the Weber number, δ_m is the mass median particle diameter, d_0 is the diameter of the metal stream, v_m is the kinematic viscosity of liquid metal, v_g is the kinematic viscosity of the atomizing medium, M/A is the mass flow rate to gas, K is a constant.

Data from source [58] for various metals are depicted graphically on log/log scale in Figure 5.34 and show consistent agreement with experimental data.

Various other empirical equations have been published.

Miller and Giles [12] have analyzed the atomization of a variety of metals and conclude that acceleration wave break-up predominates at high gas velocity. They define a modified Weber number and correlate it to material properties and the ratio of gas-to-metal mass flow rates. The functional (dimensionless) form of the relationship was obtained from experiments.

Some empirical relationships can be transformed in terms of physical models for droplet formation. That referred to as maximum stability criterion, for instance, gives maximum drop size as a function of surface tension of the liquid metal (σ), gas density (ρ_g) and velocity (v) of the atomizing medium as:

$$\delta_{crit} = \frac{\sigma}{\rho_g v^2} \tag{20}$$

This equation applies to the breakup of ligaments [42]. Secondary disintegration into particles smaller than δ_{crit} occurs only if the dynamic pressure due to the gas stream velocity exceeds the restarting force of surface tension. Owing primarily to the higher surface tension of liquid metals, energy requirements and, therefore, gas pressures used for atomizing metals is typically between 0.35 and 2.75 MPa.

Similar to water atomization, commercial gas-atomization units exhibit non-uniformly operating characteristics. Proprietary empirical relations have been established between operating conditions, material properties and powder characteristics, in particular, median particle size and standard deviation. Beddov [19] has annotated several of these empirical relations for gas atomization.

The majority of gas-atomized powders are spherical or near-spherical in shape. Small satellite particles attached to the larger particle give rise to a variable shape factor in gas atomization. The satellites are caused by collision between particles in flight and the incidence of this effect increases as overall powder size decreases due to the fine particles drown up into the atomizing zone [60].

In the absence of impurity effects and surface oxide films, particle shape is controlled by the relative magnitudes of the times for solidification and spheroidization, provided the residence time of the particle in suspended solid state in the gas is greater than either of these times. Models of both phenomena are given in [61].

In the model for solidification time in gas atomization, it was assumed that the molten droplets did not undercool, that the relative velocity between the gas phase and the particle is constant and that convective heat transfer is dominant [42]. Then, the total solidification time t_{sol} (in seconds) [42, 61] is expressed by:

$$t_{sol} = \frac{\delta_m \rho_m}{6h_g}\left[(c_p)_m \ln\left(\frac{t_{in}-t_g}{t_m-t_g}\right)+\left(\frac{\Delta H_m}{t_m-t_g}\right)\right] \tag{21}$$

where δ_m is the mass median particle diameter (m), h_g is the convective heat transfer coefficient of the gas (W/(m^2°C)), ρ_m is the density of the liquid metal (kg/m^3), $(c_p)_m$ is the heat capacity of the liquid metal (J/(kg°C)), t_{in} is the initial temperature of the particle (°C), t_g is the gas temperature (°C), t_m is the melting

point of the metal/liquidus temperature for alloys (°C), ΔH_m is the latent heat of fusion of the metal (J/kg).

The value of h_g is given by:

$$h_g = \frac{k_g}{\delta_m}(2.0 + 0.6Re^{0.5}Pr^{0.33}) \quad (22)$$

where k_g is the thermal conductivity of the gas (W/(m°C)), *Re* is the Reynolds number relative to the particle, *Pr* is the Prandtl number for the gas.

Under the influence of surface tension forces alone, the time for spheroidization t_{sph} is expressed by:

$$t_{sph} = \frac{3}{4}\frac{\pi^2\mu_m}{V\sigma_m}(r^4 - r_{tr}^4) \quad (23)$$

where μ_m is the dynamic viscosity of the liquid metal (Pa·s), V is the particle volume (m^3), σ_m is the surface tension of the liquid metal (N/m), r is the radius of spheroidized droplet (m), r_{tr} is the metal liquid trickle radius before transformation to spherical droplets (m).

A more detailed and general model to estimate the time for spheroidization of a droplet has been given by Rao and Tallmadge [62]. Lawley [15] notes that their predicted spheroidization times are not significantly different from those given by Eqn (23).

Based on these models, See and Johnston [42] have calculated the times for spheroidization and solidification of a range of droplet sizes (149–420 μm) for tin. Spheroidization times ($<2 \times 10^{-5}$ s) lower than the times required for solidification, so that only spherical particles should be produced in gas atomization, if there are no factors which hinder this transformation. The presence of ligament-shaped particles of Sn, particularly at small particle size fractions, is attributed to the presence of an oxide layer (SnO_2) which opposes the action of the surface tension.

The surface of gas atomized powders is generally smooth. The particle surfaces frequently exhibit a cellular or dendritic morphology, subject to cooling rate during solidification of the droplets. When reactive elements are prealloyed with the base elements, some surface oxidation can occur during gas atomization.

The spherical shape and smooth surface inhibit the development of green strength in cold compaction. In addition, prealloying before atomization increases particle hardness and strength which reduces compressibility. These inherent limitations of gas-atomized powders have stimulated development of elevated temperature consolidation processes to achieve high density: examples include hot extrusion and hot pressing. It is possible, by increasing the cooling rate via decrease in particle size, to change particle shape towards non-sphericity. It is also possible to add elements that alter the surface tension values (Li, Mg, Si, Ca, Mn, etc.).

The relatively high cooling rates intrinsic to gas atomization result in fine-scale microstructures. In NiAl and Ni_3Al powders, sonic gas atomized using nitrogen produced either dendritic or equiaxed structures depending on the particle size and consequently on the cooling rate [63]. The $Al_{82}Ni_{10}Y_8$ alloy powder produced in a close-coupled nozzle atomizer unit at 3.03 MPa argon jet pressure has perfectly spherical and smooth particles (Figure 5.35). In particles of several micrometers the dendritic and cellular microstructures were not detected and they tend to be amorphous (Figure 5.36).

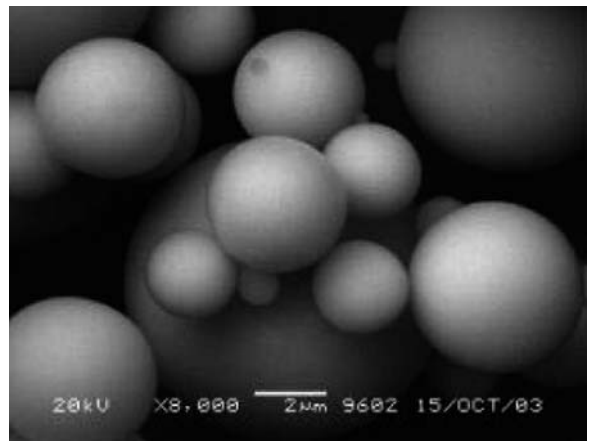

Figure 5.35 Surface morphology of $Al_{82}Ni_{10}Y_8$ alloy powder with particle diameter below 15 μm. (Source: Ref 64®)

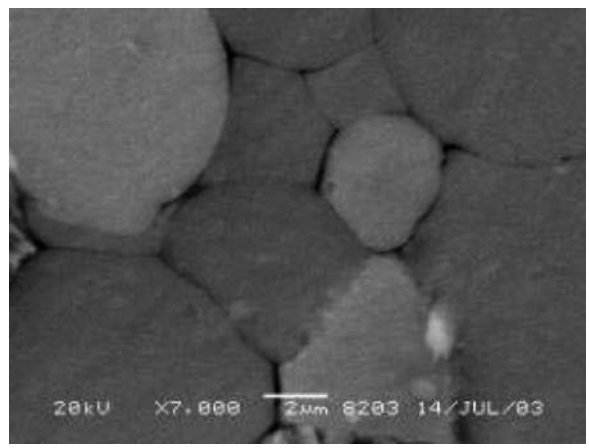

Figure 5.36 SEM microstructure of $Al_{82}Ni_{10}Y_8$ alloy powder with particle diameter below 15 μm. (Source: Ref 64®)

Internal pores can be present in gas atomized powder and may be detrimental in several respects. The effect of closed porosity leads to reduced apparent density, causes gas bubbling in thermal spray deposits and gives rise to uncontrolled dimensional change during sintering. Internal pores are of most concern in superalloy powders atomized with argon. The argon in the pores is insoluble in the alloy and this gives rise to the phenomenon of thermally induced porosity following densification by hot isostatic pressing with attendant decrease in the mechanical properties. From the study [65], it is concluded that internal closed porosity is a common phenomenon in gas atomization and that its extent increases with increasing particle size. A major source of internal porosity is gas entrapment, especially when the gas is insoluble in the solid powder particles.

Powder Cleanliness

Impurity control is of paramount importance for high-performance applications. Powder cleanliness is a major concern with atomized specialty alloys. These alloys are used frequently in applications with exacting combinations of strength, ductility, toughness and fatigue resistance. In these conditions, there are non-metallic inclusions in the powder that limit performance when the powder is consolidated. Inclusions may be introduced during melting and inert gas atomization; their source is the refractory tundish or pouring nozzle used in conventional gas atomization. The inclusions act as sites of stress concentration and can result in the initiation of fatigue cracks. This effect is of prime concern in components for aircraft engine applications.

Using practicable induction melting technique, it is possible to replicate closely the composition of the melt stock in the resulting gas-atomized powder. Thus, specialty alloys based on aluminum, copper, nickel, cobalt and titanium can be gas-atomized to exacting compositional specifications. Partial loss of elements with a high vapor pressure or reactive elements can be quantitatively compensated for during melting prior to atomization. Primary sources of intermediate impurities are initial charge impurities, the melting atmosphere, the atomizing gas and refractory ceramics (crucible, tundish and tundish nozzle). In the case of the most critical superalloys, a bottom pouring electroslag remelting furnace that discharges using a ceramic-free pouring nozzle to minimize all possibility of inclusion pickup [66] has been developed. In the EIGA (Electrode Induction Melting Gas Atomization) process [67], prealloyed rods as an electrode are inductively melted without a crucible. The metal liquid droplets from the electrode fall into the atomization nozzle design and are atomized with an inert gas jet. The EIGA process is used for titanium and niobium alloy powder production [68] and can also be applied to other alloys. Process developments in EIGA technique [69] allow this process to be conducted crucible- and ceramic-free, with larger electrode diameters up to 61 mm and increased melt flow rates of 26.4 kg/h. The optimized technique was applied for the atomization of pure Ti, Ti–6Al–7Nb and gamma-TiAl-based Ti–46Al–9Nb alloy powders. The oxygen level of the Ti–6Al–7Nb rod was about 1800 ppm; for the argon atomized powder, fraction $<20\,\mu m$, the oxygen content increases to 2300 ppm. The TiAl rod had an oxygen level of 560 ppm; for powder fraction 63–90 μm this level was maintained.

The control of the level of interstitial is very important, particularly in titanium alloys, titanium aluminides and beryllium. The control of interstitial levels in titanium alloys and aluminides is particularly important because ductility is very sensitive to carbon, oxygen, nitrogen and hydrogen impurities. Typical interstitial impurity contents of gas-atomized gamma titanium aluminide, alpha two titanium aluminide and alpha titanium alloy powders are given in Table 5.4. There is, in the main, no increase in carbon, nitrogen and hydrogen over the starting material during atomization. The increase in oxygen content from the starting material to the $<500\,\mu m$ powder is typically 200 ppm [42,70]. Nitrogen content appears

Table 5.4 Typical interstitial impurity contents of gas-atomized gamma titanium aluminide, alpha two titanium aluminide and alpha titanium alloy powders

Alloy	Impurity elements, ppm (weight)			
	Carbon	Oxygen	Nitrogen	Hydrogen
Gamma titanium aluminide	200	800	50	20
Alpha two titanium aluminide	200	800	50	50
Alpha titanium alloys	200	800	50	75

(Source: Ref 12 and Ref 70)

to be independent of particle size but the oxygen content shows an increase from 800 ppm in $<500\,\mu m$ powder to 1020 ppm in $<45\,\mu m$ powder due to the large increase in surface area.

In helium-atomized beryllium powder, it is possible to keep the oxide content to a relatively low level [12, 71].

Other Gas Atomization Methods

Internal Mixing Nozzles

In an internal mixing atomizer, gas and liquid metal are mixed under pressure and expansion and atomization occur at the nozzle exit into the chamber [72]. As is shown (Figure 5.37), the gas enters with high velocity through tangential inlets into a nozzle to which the liquid metal flows axially and is carried by the rotational gas flow in film form on the inner surface of the nozzle walls to the outlet in the bottom. The narrowing of the lower nozzle part forces the gas to accelerate so that the liquid film becomes thinner. At the outlet, the film breaks into small droplets. Concerning its working principle this nozzle design is termed a prefilming spin nozzle (PFSN). The lab melt feeding unit allowed the control of melt flow rates between 0.4 and 5 ml/min for temperatures up to 200°C. The atomization conditions were as follows: atomizing gas was argon, gas pressure max 0.6 MPa and initial metal was 62Bi–38Sn (weight). Its physical data were as follows: melting point 144°C, viscosity 2.2 mPa s at 200°C, surface tension 0.41 N/m at 150°C, density 8.7 g/m^3. The average particle diameters range from 14 to 25 μm.

The pressure swirl hybrid prefilming atomizer described above (see Figure 5.26), contains an internal mixing nozzle in combination with ring gas atomizer.

The fundamental disadvantage of the internal mixing technique is the engineering difficulty of arranging to pressurize the melt to the same pressure as the gas. There are also problems with erosion of the ceramic nozzles employed because of the metal velocity, normally only 1–3 m/s in a pouring nozzle could be expected to rise to the same order of magnitude as the gas velocities, i.e. possibly about 100 m/s. Thus, applications are so far very limited.

Soluble-Gas-Atomization Process

The soluble-gas-atomization process is also known as vacuum atomization (see Figure 5.1(h)). This process [73] is based on the rapid expansion of gas-saturated molten metal, resulting in a fine atomization of molten droplets that form as the dissolved gas, usually hydrogen or an argon hydrogen mixture, is suddenly released in an evacuated powder collection tank (Figure 5.38). The droplets solidify at a rate of about 1000°C/s. The powder collection tank is cooled under vacuum, powder is sealed and then backfilled with an inert gas. This technique is capable of atomizating up to 1000 kg of superalloy in one fusion and produces spherical powder. This process has been employed in commercial scale for LC Astroloy, MERL 76 and IN-100 production.

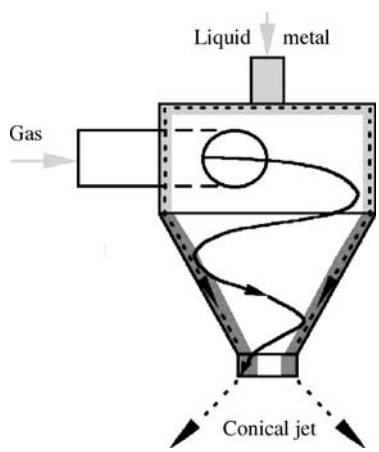

Figure 5.37 Principle of the internal mixing nozzle.

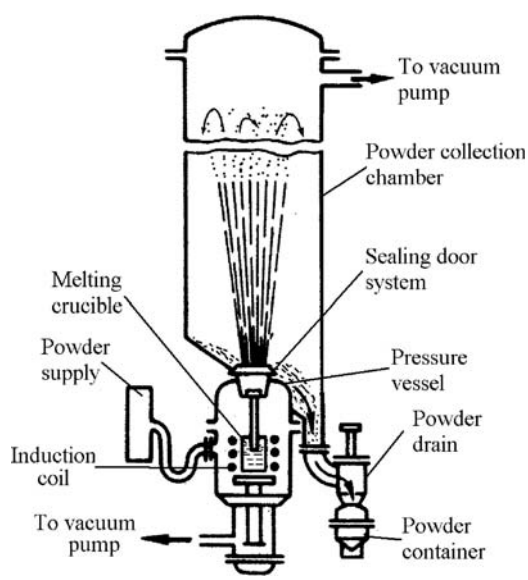

Figure 5.38 Soluble gas atomization system.

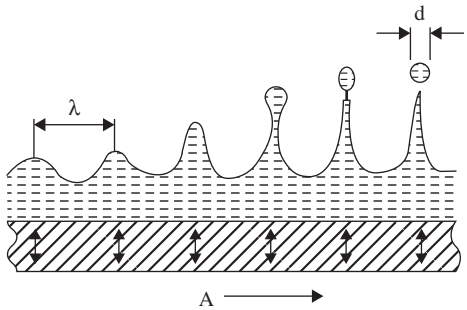

Figure 5.39 Capillary wave atomization model.

Ultrasonic Gas Atomization

Lierke and Griesshammer seem to have been first to report the experimental production of metal powders by ultrasonic atomization in 1967 [74]. Later, they achieved atomization of silver [75]. Many experimental studies have been carried out to evaluate particle size distributions. There are differences between low-frequency (20–100 kHz) and high-frequency (up to 3 MHz) atomizers. Analytical studies work on two assumptions: either the breakup mechanism results from growing instabilities in a capillary wave pattern created at the surface of the liquid film, or it derives from cavitational phenomena [76].

According to the capillary-wave hypothesis (Figure 5.39), a thin layer of a liquid wetting the surface of a solid resonator that vibrates vertically to its surface plan, forms a chessboard-like pattern of stationary capillary waves. This occurs when the vibration amplitude exceeds a threshold value. On further increase of the amplitude, ligament breakup of the liquid follows and droplets are hurled from the crests of the capillary waves. The parameter of interest is λ, the capillary wavelength.

Rayleigh [77] stated that

$$\lambda = \left(\frac{2\pi\sigma}{\rho v^2} \right)^{1/3} \tag{24}$$

where σ is the liquid surface tension, ρ is the liquid density, and v is the oscillation frequency, if the oscillation frequency in the liquid is half that in the solid resonator then

$$\lambda = \left(\frac{8\pi\sigma}{\rho f^2} \right)^{1/3} \tag{25}$$

where f is the ultrasonic frequency.

Later Ruthardt and Lierke [75] measured the particle diameter amounting to 0.25 λ for silver.

Theoretical predictions based on the capillary-wave hypothesis are numerous and essentially apply to low-frequency, low-flow-rate atomizers, whereas cavitation is supposed to occur at higher regimes [76,78]. Yule [79,80] has shown that capillary-wave atomization is not as orderly as foreseen theoretically. As an alternative, Dumouchel and Boyaval [81] used the maximum entropy formalism (MEF) to model size distribution. A detailed description of the MEF can be found in Kapur's paper [82]. In general, the MEF is a mathematical tool for the elaboration of probability distributions.

On HEV's (University of Applied Sciences of Western Switzerland) ultrasonic atomizer [29], magnesium alloy, AZ63 and pure silver were atomized at 20 kHz. Atomizer, induction melting unit, transfer tube, transducer and tubular resonator are the principal parts of HEV's ultrasonic atomizer. Experimental results show a spheroidal particle shape (Figure 5.40); the powder fraction $<50\,\mu m$ yields are about 65 and 71 vol% for magnesium alloy and silver powders, accordingly.

No commercial operator is known to use this method and the largest melter used has been in the 10–50 kg size range.

Hot Gas Atomization

In practice, the hot gas process has been partly motivated by an appreciation of the fact that it allowed the production of finer powders, and partly by the fact that it reduced or avoided the problems of nozzle freezing when processing lower melting point alloys (e.g. Li, Sn, Bi, Cd, Pb, Zn and Al). This allows the use of smaller nozzles and pouring rates which, in turn, allows convenient continuous production as well as the production of finer powders than is possible at higher melt flow rates.

The effect of gas temperature on particle size is shown in Figure 5.41. These data are the result of computation [83] based on dependence of the decrease in the median size of the powder on the square root of gas absolute temperature. In this case, a gas temperature of 200°C reduces the size by 11% and 400°C by 19%. The effect of gas temperature on gas consumption for a constant particle size is shown in Figure 5.42.

A calculation of the economic effect in the case of steel powder production [83] shows that going from 20°C to 200°C reduces costs by 16% and 400°C by 34% (this calculation assumes a gas cost of 0.14 €/m^3 for nitrogen and electricity cost for heating of 0.14 €/kWh). Heating gas to 200°C or even 400°C is not very demanding technically, while to reach 1000°C is far more difficult. Besides that,

savings from going from 499°C to 1000°C are only a further 18%.

Hot gas atomization was applied for the production of inexpensive copper powder for metal injection molding (MIM) where powder costs currently form a high component part [2]. The powder with median diameter about 10 μm was produced by the following process parameters: pouring temperature 1400°C (melting point 1083°C) and atomization gas temperature 500°C.

However, hot gas atomization leads to an increase in the time needed for solidification rather than to a decrease in median diameter and that necessitates an increase in the size of the atomizer chamber. The cooling rate decrease adversely affects the possibility of creating advanced nanostructure alloys.

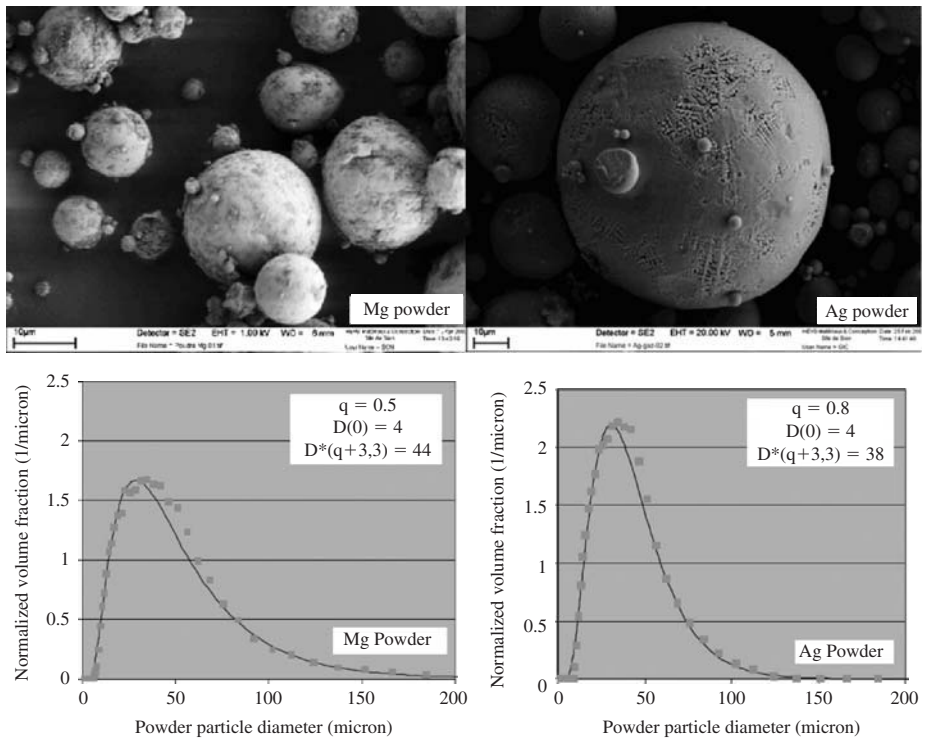

Figure 5.40 Scanning electron micrographs of the ultrasonic atomized magnesium alloy and silver powders and their size distribution. (Source: Ref 29)

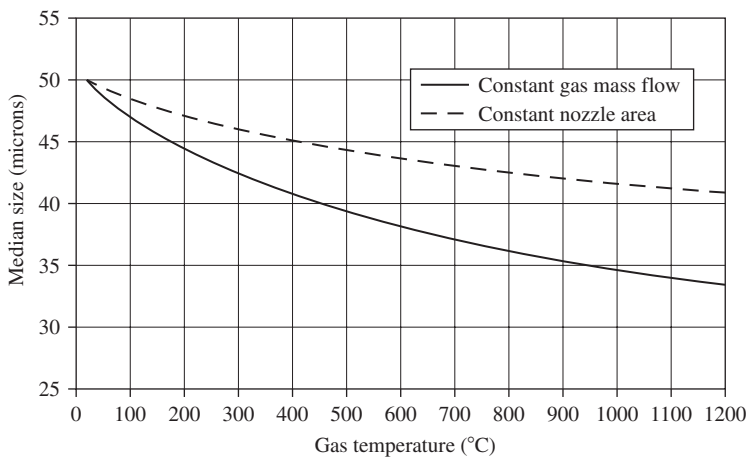

Figure 5.41 Effect of gas temperature on particle size. (Source: Ref 83)

Liquefied Gas Atomization

The atomization of melts with liquefied, cryogenic gases seems to have been developed in 1988 [84]. The so-termed liquefied gas-atomization (LGA) is, in principle, similar to the well-established water-atomization technique (WA) and results in comparable or even higher cooling rates than WA. During LGA no oxidation occurs between the atomizing fluid and melt. Materials exhibiting high sensitivity to oxidation have been atomized via LGA, such as the rare earth NdFeB [85] and NiLa or special solder alloys. Starting with atomizing arrangements similar to WA (free-fall design), the technique has been further developed for the use of confined nozzles, similar or identical to the one used for gas atomization (GA).

Two identical inert gas atomization units at ATZ-EVUS, a laboratory unit up to 30 kg and a pilot unit 100 kg per batch have been used for GA and LGA powder production [86]. Melting is done by inductive heating. The melt orifice diameters range from 1.7 up to 4 mm, the melt superheat temperatures are typically 100–200°C, the atomizing pressures range from 1.0 to 25 MPa. Liquefied gas after cooling to cryogenic temperatures flows to the atomizer when the flow of the superheated melt begins. The mass median diameters range from 30 to 80 μm for NdFeB alloy, copper and Sn–37Pb alloy. The cooling rate achieved is $>10^6$ °C/s in the above laboratory size unit by melt flow rates up to 20 kg/minute [85].

No commercial operator is known to use this method. More detailed data, including powder characteristics, economic effect, and safety engineering aspects, are necessary to evaluate liquefied-gas-atomization process.

Centrifugal Atomization

Models of Centrifugal Atomization

According to the studies of Hinze [87], Tanasawa [88], Champagne and Angers [89, 90] and Halada [91], in centrifugal atomization, there are three basic droplet formation modes. These models conform to the rotating electrode process and are shown in Figure 5.43. Their analysis is applicable to centrifugal atomization in general.

The direct drop formation (DDF) mode occurs at relatively small rotating speeds and small rates of liquid supply. In this mode, a lot of protuberances grow

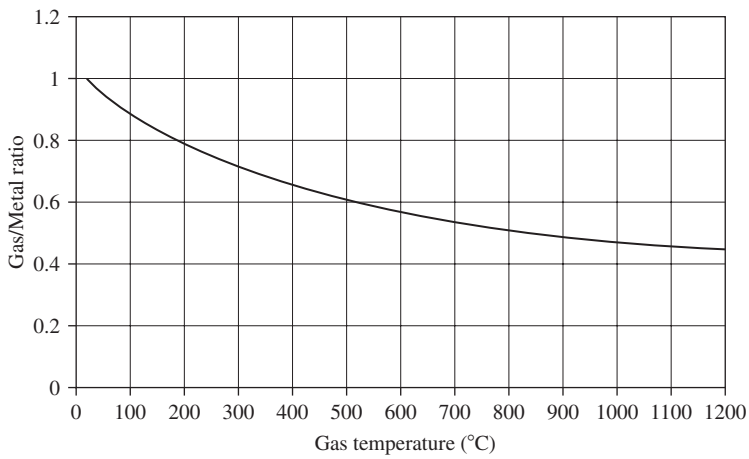

Figure 5.42 Effect of gas temperature on gas consumption for constant particle size. (Source: Ref 83)

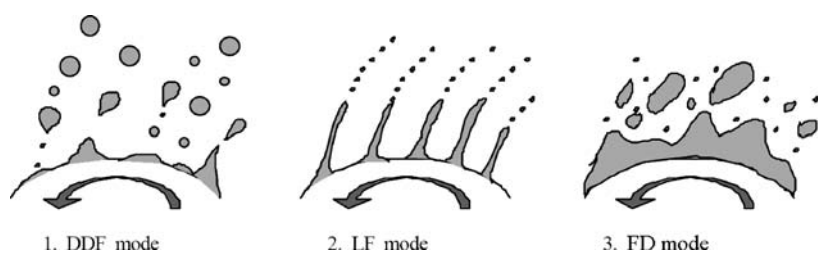

Figure 5.43 Three disintegration modes in centrifugal atomization.

under the balance between centrifugal force and surface tension. When surface tension is lower than the centrifugal force, droplets are separated and ejected from the protuberances. The major part of every protuberance form the main drops in large sizes. Its tail usually becomes satellites. Therefore, the typical powder size distribution in this mode has two peaks with equal numbers of large and small droplets.

The ligament formation mode (LF) occurs when the rate of supply of molten metal at the periphery of the electrode increases. Here the protuberances develop larger amplitude than in the DDP mode before Rayleigh instability breaks up the elongated ligaments. Droplet size increases and, though still bimodal, the weight fractions of the small and large droplets become similar as the liquid supply rate increases.

When the liquid flow rates are very high, ligaments become unstable and the disintegration mode changes gradually to formation disintegration (FD). The transition conditions among these modes had been studied experimentally in a broad range: $10^3 < We < 10^7$ and $10^2 < Re < 10^6$ by Masumoto [92]. The condition range for metal centrifugal atomization is Weber number: 10^4–10^5 and Reynolds number: 10^5–10^6.

Champagne and Angers [89,90] observe that for various metals (e.g. Al, Cu and Zn), the final droplet shape seen in the DDF mode is spherical. In the LF mode a more ellipsoidal shape is formed.

Champagne and Angers [89,90] discovered that the ratio of two parameters determines the transitions from the DDF to the LF and LF to the FD modes:

$$X = \frac{\left(\dfrac{Q\omega^{0.60}}{D^{0.68}}\right)}{\left(\dfrac{\sigma^{0.88}}{\eta_L^{0.17}\rho_L^{0.71}}\right)} \tag{26}$$

where Q is the liquid supply rate (m^3/s), ω is the angular velocity of the anode (rad/s), D is the anode diameter (m), σ is the surface tension (N/m}, η_L is the dynamic liquid metal viscosity (Pa s), and ρ_L is the density of the liquid (kg/m^3).

The numerator includes only process variables while the denominator includes only the material variables. Using the above units for the process and material variables, the DDF to LF mode change occurs when $X = 0.07$. The second mode change to FD mode occurs when $X = 1.33$. These relations are plotted in Figure 5.44. Thus, an increase in melting rate and angular velocity and decrease in rotating anode diameter favor a transition from the DDF to the LF mode and finally to the FD mode. Close agreement exists between model predictions of the transitions in atomization modes for various metals (Figure 5.44).

Centrifugal atomization generally leads to a narrower spread in particle size than does gas atomization. The analysis of centrifugal atomization developed by Champagne and Angers allows for a quantitative prediction of mean particle diameter in the direct droplet formation mode. In its present form, the model gives no indication of the extent of droplet sizes.

The median particle size d_{50} for the rotating electrode process is approximately defined [93] by

$$d_{50} = \frac{K}{\omega\sqrt{D}} \tag{27}$$

where K is a constant for a given alloy for a limited range of arc power.

In a simple model [94], which considers force balance between centrifugal force and surface tension forces, the particle size is expressed as:

$$d = \sqrt{\frac{A\sigma}{\rho_m\omega^2 R}} \tag{28}$$

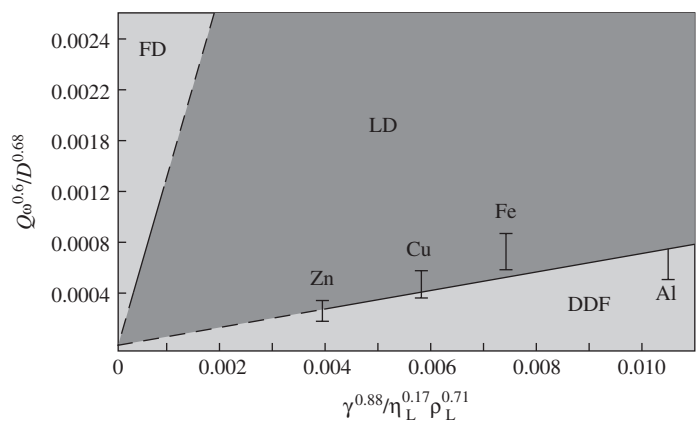

Figure 5.44 Atomization mechanism domains in centrifugal atomization. (Source: 12)

where ω is the angular velocity (rad/s) of the rotating disc (or the electrode), R is the radius of the atomizer (or electrode) (m), ρ_m is the liquid density (kg/m^3) and σ is the surface tension (N/m). A is a constant with value 6 [95] in the elementary case (spheroidal particle shape).

Actual powder sizes are coarser then those predicted [76], which may be explained by the influence of viscosity, particularly at higher speeds. In effect, the molten film is 'slipping' on the disc surface, making its speed less than the peripheral speed of the disc. If a term that is counteracting the centrifugal acceleration, and that includes both the viscosity and the speed at the rim of the disk, is added to the basic model (Eqn 28), the following relationship is suggested by Tornberg [37]:

$$d = \sqrt{\frac{A\sigma}{\rho_m \omega^2 R(1 - (\omega R)^n \eta)}} \qquad (29)$$

where the constant $A = 4.8$ and the exponent $n = 0.93$.

Centrifugal Atomization Methods

There are several different types of centrifugal atomization process (see Figure 5.1) which are discussed. In general, centrifugal atomization methods are far more energy-efficient than gas and water atomization, where only about 1% of the jet energy is used in the disintegration of the metal stream [12]. In contrast, the energy used in centrifugal methods is low as it all goes into acceleration of the metal droplets instead of into atomizing fluid, as in the case of two-fluid techniques. Centrifugal atomization also generally leads to a narrower spread in particle size than does gas atomization (see Figure 5.2), with σ_g as low as about 1.2 in some cases.

As the process depends on the solution to the problem of finding a compatible material for the spinning disk or cup, the applications that have been, and are currently, used on a significant industrial scale are quite distinct.

Spinning Disc Atomization

Solder powder for electronic applications has a very demanding specification: it must be perfectly spherical and satellite-free, it must be very low in oxygen content (≈100 ppm), and it must have a very narrow size distribution. In 1997, more than half of the demand was for size grade that is nominally −45 + 25 μm. Attempts to make this product with inert gas atomization have practically ceased as yields are as little as 5% and the avoidance of satellites is very difficult.

In the USA, Europe and Japan, there are many producers using spinning disc methods to make this product. This is possible because a steel disk is well wetted by ordinary Sn63Pb37 solder and is not very quickly eroded. A disk with diameter of 40–100 mm running at speeds of 30 000–60 000 rpm can produce this material with good yields of 30–70% and at rates of 50–100 kg/h. Annual production is probably several thousand tonnes per year.

When used with higher melting point metals, it is difficult to run at the level of speeds that are used on solder, because of the need to increase the plant diameter. However, there are markets for coarser powders of zinc (alkaline batteries), aluminum (chemical) and magnesium (flares) that are made by this process. In all cases, the cup is 100–200 mm diameter, running at moderately high speeds, from 3000 to 10 000 rpm. The chamber size needed is very large, up to 12 m in diameter, but productivity can be very high. Battery applications commonly require −600 + 100 μm zinc powder. Using a 5 kW spinning cup, 98% can be achieved, at outputs of several tonnes per hour, and with compressed air costs.

Course aluminum powder is also produced in this way but, because the large size of plant needed freezes large droplets, it is done in the open air, which produces a needle-shaped powder. In this case, a perforated steel or cast iron cup is used to make a series of streams of metal, which break up into needles due to the oxide film on them. Production is probably thousands of tonnes per year.

The spinning cup water granulation process [96] allows an increase in the cooling rate and notable decrease of the size of plant owing to cooling the molten droplets in water. Thus, the chiller chamber size is only 1.2–1.5 m in diameter in comparison with 12 m in diameter in open air granulation. Chapter 13 includes more detailed information about this technique.

Rapid Solidification Rate (RSR) Process

RSR process is another design of centrifugal disk or cup atomization, which was developed for superalloy powder production. To overcome the problems of the material in handling high melting and aggressive alloys, the process [97] employs a high-speed water-cooled rotating disk (20 000–50 000 rpm), which breaks up the molten metal stream. To enhance solidification rates, the resulting droplets are then struck by high-pressure helium gas as they leave the periphery of the rotating disk. Powders produced by the RSR

process are spherical, satellite-free and have smooth surfaces. Particle sizes are usually below about 200 μm with a mass median particle diameter <90 μm and a low standard deviation in the range 1.4–1.6.

RSR facilities currently in use incorporate closed-loop helium recirculation. Based on Ni-base alloys, the largest unit has a melt capacity of about 900 kg with an atomization chamber close to 5 m in diameter. In the intermediate size unit, melt sizes are 135 kg with an atomization chamber of about 2.3 m in diameter. Production rates can be varied between 0.05 and 0.3 kg/s, for Ni-base alloys. Typically, RSR droplets smaller than 100 μm in diameter cool at rates of about 10^5°C/s. Apart from these operating variables, the superheat of the melt has a strong influence on particle size and hence particle cooling rate.

More detailed data can be found in Chapters 13 and 14.

Melt Spinning Roller Technique

At present, maximum melt cooling rate has been achieved under heat abstraction from a melt by means of a contact with metallic substrate. The main conditions for advance of high melt cooling rate due to heat conductivity are the following:

- minimal loss of heat during carrying from furnace to cooling point
- minimal melt thickness in the line of heat sink
- high heat conductivity of freezing metallic material (substrate)
- sufficiently high melting point of the substrate
- good heat contact (first of all cleanness of the substrate surface) of the freezing and cooling materials.

As freezing material, pure copper or its alloys (e.g. beryllium bronze) mostly serve. For good heat contact, the substrate surface is thoroughly polished. The most advanced method of obtaining particles (ribbons, flakes) by means of their freezing on a substrate is the spinning roller technique [96]. A liquid metal stream (Figure 5.45) collides with surface of a rapidly rotating roller and wets it. At the contact point a liquid metal bath is formed. The moving roller surface expands the bath into a ribbon, which begins to move with the same velocity as that of the roller surface. The solidified ribbon is then released from the roller under the action of centrifugal force.

The cooling rate of liquid metals achieves 10^5 – 10^7°C/s depending on ribbon thickness, which is changed from 20 to 80 μm; the roller circumferential speed is ≈30 m/s [94], output of the Al alloy is 4–6 kg/minute.

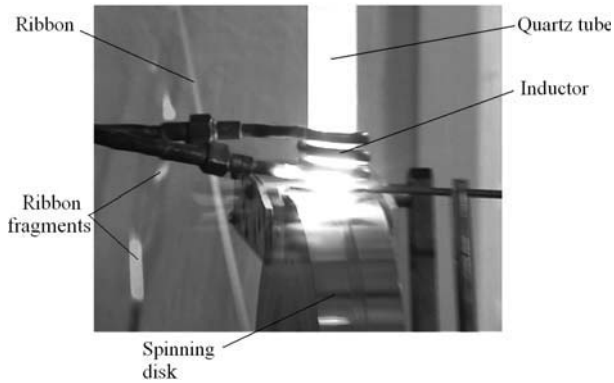

Figure 5.45 Aluminum alloy ribbon obtaining on melt spinning roller. Courtesy of IPMS.

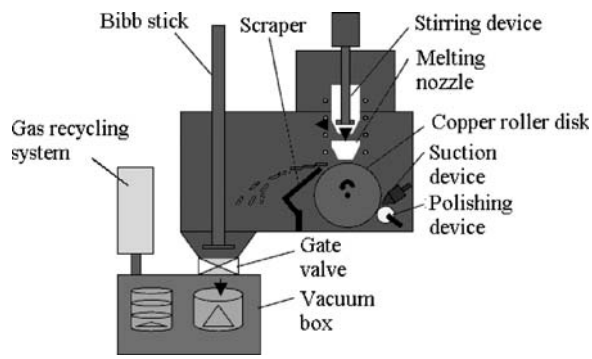

Figure 5.46 The diagram of flaky powder production by melt spinning roller technique.

The phenomenon of heightened solubility becomes possible by such cooling rates. Thus, for example, in aluminum alloy ribbons an increase of the non-equilibrium solubility of scandium up to 2 wt% was achieved [98]. Alloying of aluminum with scandium leads to hardnesses of 950, 1200 and 1800 MPa for scandium concentrations of 0.6, 1.0, and 2.0 wt%, respectively (significantly higher than the maximum hardness achieved for aluminum alloys by traditional technology, i.e. 800 MPa).

At the plant shown in Figure 5.46, a flaky magnesium powder is manufactured [99]. $Mg_{97}Zn_1Y_2$ alloy was melted by high-frequency induction heating in an argon atmosphere and flaky powder was produced by spinning roller atomization. In the experiments, the distance between the melt nozzle end and copper roller surface was 0.3, 15, and 30 mm, while the roller circumferential speed was 30, 40, and 50 m/s. As a result, the flaky powders are produced in the range from 20 to 65 μm and Vickers hardness from 104 to 134 depending on experimental conditions.

The melt spinning roller technique is widely used in laboratory investigations, but no commercial operator is known to use this method.

Rotating Electrode Atomization

In the rotating electrode process (REP), one end of a metal bar is melted while it is rotated around its longitudinal axis (see Figure 5.1). The molten metal is ejected by centrifugal force in the form of droplets from the periphery of the bar. The REP process was developed by Nuclear Metals, Inc. and patented [100,101].

In the original process, the consumable rotating bar is the anode of a direct current power circuit and the permanent (non-melted) stationary cathode is either a cooled tungsten tipped device or a transferred arc plasma torch. When the later mode is used to melt the end of the rotating anode, the atomization process is termed the plasma rotating electrode process (PREP). A chamber of 2440 mm in diameter is used with the circular section oriented. Anode rotational speeds are normally 1570 rad/s. Melting of the anode is conducted in an inert atmosphere. Helium gas enhances both arc stability and the convective cooling efficiency of the atomized droplets.

Powder particles produced by REP and PREP are spherical with smooth high quality surfaces. The particle size range is typically from 50 to 400 μm with a mass median particle size around 200 μm [12]. Particle cooling rates are lower than in water or gas atomization. From secondary dendrite arm spacing measurements, the cooling rate is $\leq 10^2$°C/s, depending on the gas in the chamber and the particle size.

However, a major drawback is the mechanical limitations on rotational speed, which limit the minimum median particle size to about 50–150 μm [3]. Also, the cost of making a high-quality bar of metal is very significant and productivity is low and energy consumption high compared with other techniques.

Other Methods

Impact Atomization

Impact atomization was developed [102] for producing rapidly solidified particulates. In this method, a molten alloy and volatile liquid coolant are fed simultaneously to a rapidly rotating impeller. As the molten alloy is atomized, the coolant vaporizes; the necessary heat of vaporization of the coolant is taken from the droplets as they solidify. Patents covering this process were issued to the Dow Corning Corporation [103,104]. Powders have been prepared from a variety of stainless steels, nickel, copper and a glass forming alloy [102]. Coolants used included water, liquid ammonia, methanol and hexane at flow rates from 60 to 200 L/minute, depending on the heat of solidification of the alloy, the heat of evaporation of the coolant, the degree of superheat and molten metal feed rate.

This process has been used in Argentina where, since 1997, two commercial plants have been operating using induction melting furnaces with 80 and 500 kg capacity, respectively [105]. Both plants include: furnace, tundish, rotating impeller, atomization tank with water, reservoir of circulating water and a pump feeding circulating water to the impeller. The speeds of impeller rotation are from 2000 to 3500 rpm depending on alloy type, required particle size distribution and powder apparent density values. The commercial bronze (Cu–5Sn–5Zn–5Pb) powder contains size fraction ≤44 μm up to 26 wt% and size fraction ≥47 μm max 20 wt%. For 2.2–2.5 t/h atomized powder yield a 10 kW belted drive is used.

Besides the industrial types of atomization processes, there are also many atomization methods with scientific potential that have been described in the literature. There are the following methods.

Vibrating Electrode Atomization

Powder is atomized at the molten end of a vibrating consumable electrode in rod form that is continuously fed between rollers into an atomization chamber. A water-cooled rotating electrode of copper or graphite is located opposite the end of the consumable electrode. The rollers are attached to an electrodynamic oscillator which transfers vibration to the rod electrode. Thus, the electrode forms a resonant rod with one free and one fixed end. Atomization takes place in an inert atmosphere when the arc is struck between the rotating electrode and the vibrating end of the rod electrode.

In the facility described in the literature [106], currents between 600 and 1200 A were generated at a potential between 30 and 60 V. Electrode vibration frequencies up to 500 Hz were evaluated. Powder particles are spherical with mass median sizes typically in the range 300–500 μm. Vibrating rod diameter range is 1–4 mm and feed rate 1.7–4.3 m/minute. Disadvantages of the vibrating electrode atomization are that particles are coarse, productivity is low and cost high.

Melt Drop Orifice Technique

There are several types of such technique, which include impulse atomization (IA), melt drop vibrating orifice method and pulsated orifice ejection method.

Impulse Atomization Method

A schematic of the process is shown in Figure 5.1(g). This unit includes the impulse generator, the mechanical drive, a tundish and a nozzle plate complete with orifices [107]. There are two modes of impulse atomization operation: the first (gravity impulse mode) is the generation of monosized granules larger than 1 mm in diameter and the second (impulse mode) is the atomization of droplets with a narrow size distribution less than 1 mm up to 150–180 μm. In the impulse mode of operation, by varying the plunger acceleration, orifice size, orifice shape, melt superheat temperature and type of gas atmosphere, the powder particle sizes and distribution, shape and microstructure can be controlled to the required specifications. In gravity impulse mode, the melt stream free falls out through the orifice and impulses are applied to generate millimeter-sized droplets. The powders have been produced in an experimental tower 0.5 m in diameter and 4 m in height. In the atomization chamber, the quiescent gas atmosphere into which the melt has been atomized includes helium, nitrogen, argon and air. The nozzle plate contained over 500 orifices. Standard refractory materials are used for the tundish, plunger and orifice plate. There are no temperature limitations to the use of impulse atomization provided an appropriate refractory material is available for use. For example, a nickel–aluminum alloy was atomized at 1600°C.

Table 5.5 includes a summary of the materials and range of particle sizes reported in [107]. The powders have a narrow particle size distribution; the standard deviation (δ_{84}/δ_{50}) range is $1.1 \leq \pi \leq 1.6$, typically 1.4, for the impulse mode.

In the impulse mode of operation, mass flow rates of 225 kg/h have been attained in pilot scale tests with, to date, 2.5 h of continuous operation with zinc. This corresponds to a mass throughput of 7300 kg/(m^2 s) based on the area of orifices in the nozzle plate; while the mass throughput for aluminum range in these experiments from 2000 to 3000 kg/($m^2 \cdot$ s). The mass flow rate attained with the gravity impulse mode was 15 kg/h for 2 mm magnesium granules. Alcoa has developed a forecast model for the conversion cost of a commercial gravity impulse unit [107].

Table 5.5 Powders and granules produced using impulse atomization method

Metal or alloy	Atomization mode	Average particle sizes	
		Unit	Volume
Aluminum	Impulse mode	μm	310
Aluminum	Gravity impulse mode	mm	2–10
Al–(5–24 wt%)Cu alloys	Impulse mode	μm	250–710
Al 6061 and Al 6111 alloys	Impulse mode	μm	250–850
Al 357 alloy	Impulse mode	μm	560–700
Al–(0.1–8.0 wt%)Fe alloys	Impulse mode	μm	400
Al–(10 & 24 wt%)Sr alloys	Impulse mode	μm	1000
Al–Al_2O_3 composite powders (5 to 20 vol% of 35 μm reinforcement)	Impulse mode	μm	1000
Copper	Impulse mode	μm	200–1400
Bronze 90/10 and bronze 94/6	Impulse mode	μm	180–720
Pb–(10 &12 wt%)Sn alloys	Impulse mode	μm	200–1000
Magnesium	Impulse mode	μm	850–1000
Magnesium	Gravity impulse mode	mm	2 and 4
Mg–9Al–1Zr alloy	Impulse mode	μm	850–1000
AZ91D alloy	Impulse mode	μm	850
Knife alloy	Impulse mode	μm	1000
90Ni–10Al alloy	Impulse mode	μm	350
34Ti–45Cu–1Zr–8Ni alloy	Impulse mode	μm	350
Zinc	Impulse mode	μm	150
Zn–500 ppmPb	Impulse mode	μm	250

Melt Drop Vibrating Orifice Method

In this method, molten metal contained within a closed, pressurized crucible is subjected to vibratory oscillations. Forcing the metal through a nozzle at the bottom of the crucible and into a vacuum or inert gas chamber causes it to form a jet and break up into uniform droplets. The technique has been demonstrated with aluminum, beryllium, copper, lead and some superalloys [108] and has been proposed for solder [109]. The technique was in limited industrial use in the 1990s, making precision solder balls for electronics with sizes in the range 500 to 1000 μm. It is limited as production is related to the square of particle size and nozzle blockage is a problem for orifices in the 200–20 μm range.

Pulsated Orifice Ejection Method

This method is intended for the production of monosized spherical particles [110]. Figure 5.47 shows a schematic diagram of a pulsated orifice ejection method. A piezoelectric actuator was used as a driving device of a metal diaphragm, in which the maximum displacement is 14.7 μm and the frequency is 69 kHz. Rectangular waves were generated by a function generator for controlling the output waveform of a power amplifier. A hole about 0.2 mm in diameter, as an orifice, was machined at the center of the bottom of the tundish. Each pressure pulse produced one melt droplet. The apparatus allows the preparation of particles having very narrow particle size distribution with size deviation less than 2% of mean particle size. It has been found that the pulsated orifice ejection method is applicable for preparing monosized particles of various metals and alloys. For example, the monosized Sn–3.5 wt% Ag powder with mean particle size of 187 μm with 0.8% deviation was demonstrated.

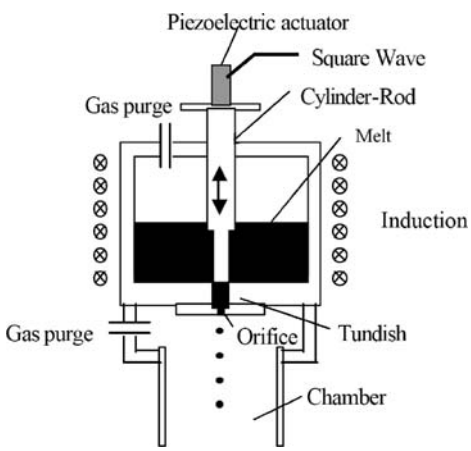

Figure 5.47 Schematic illustration of pulsated orifice ejection apparatus.

Roller Atomization

In roller atomization, a molten metal stream is fed between rapidly rotating twin rollers (see Figure 5.1(d)). Its feature is that little conductive heat transfer between the liquid metal and the rollers takes place [111]. This distinguishes roller atomization from spinning roller in which rapidly solidified ribbon or flaky particles are produced. Epoxy and phenolic resin coatings on the rollers were found to satisfy the heat transfer requirements for temperatures below 300°C, because of poor thermal stability. Epoxy/alumina roller coatings have been used for the atomization of higher melting point metals and alloys. The original atomization facility consisted of a pair of 150 mm diameter rollers contra-rotated at speeds up to 1250 rad/s with a roller gap in the range 50 to 100 μm. The process has been used to atomize a range of metals including lead, tin, aluminum and copper at metal flow rates up to 6 kg/minute. The particle shapes can be irregular, acicular, spheroidal, or flaky, depending on the operating conditions and the metal properties. The spheroidal particles are relatively coarse; mass median particle diameters for Sn powder are in the range 250 to 680 μm. Primary operating variables are roller speed, roller gap, metal flow rate, metal stream velocity and metal superheat.

Plasma Atomization Process

This process was developed to produce fine spherical titanium powder using titanium wire as the starting material [112]. The wire is fed into the apex of three plasma torches, where it is melted and atomized in an argon atmosphere. Droplets are then cooled during flight in the argon atmosphere with a cooling rate in the range 10^2–10^3 K/s and solidify, forming spherical powder particles. Spherical titanium and Ti-6Al-4V alloy powders with diameters from 5 to 150–250 μm have been produced commercially in four grades differing as to particle sizes. The oxygen content depends on particle size and is in the range 0.1–0.3 wt %. The flow rate varies depending on particle size. PyroGenesis Inc. proposes the use of plasma-atomized titanium powders for producing porous filters, applications in injection molding and thermal spray processes and biomedical applications.

Vacuum-dynamic Atomization

This method is based on the use of energy of two contrary rotating gas flows (Figure 5.48) with initiation of tornado result (USSR Patent 1,082,566, Jan., 1984). However, there are no known evaluations of vacuum level and the rapid expansion of gas-saturated molten metal.

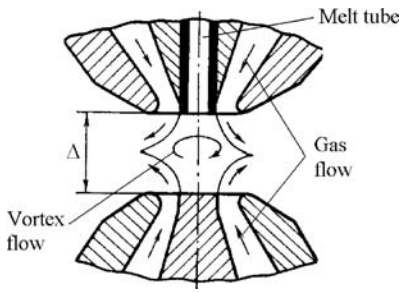

Figure 5.48 Schematic representation of vacuum-dynamic atomization.

Granulation

Granulation is a term that is used to define two dissimilar processes. In one definition, granulation is defined as the production of a metal product by atomization of molten metal. These processes have been discussed above. In the other definition, the most commonly used techniques are spray drying and spray granulation. Granulation is the purposeful agglomeration of fine particles into larger clusters to improve certain powder properties. For example, bulk powders characteristically have low density, do not readily flow, are dusty and have low thermal conductivity. When properly granulated, the same powder pours easily, exhibits a high and uniform bulk density, does not 'dust' and transfers thermal energy more efficiently.

Spray Granulation

The basic method for making granules in a fluidized bed can be by the combination of the hot gaseous fluidized bed and a two-fluid spray nozzle. A binding liquid or solution is spread onto a bed surface of fluidized particles or is sprayed directly into the bed (Figure 5.49). It tends to show that compared to seed particles, larger spray droplets generally result in the formation of agglomerates, which is influenced by variation of operating conditions. In relation to granule growth of simultaneous coating and agglomeration in a hot fluidized bed, the size distribution and growth rate of granules under continuous operation can be derived from the material balance of the bed particles. Granule size increases as the fraction of the bed exposed to the binding liquid is reduced and the spray nozzles are adjusted to give coarser droplets. Increasing the intensity of agi-tation of the bed (with of higher velocity) decreases the size of granules. There is an upper limit on granule size because of the tendency of the powder bed to defluidize. However, spray granulation can form larger granules than are usually possible by spray drying because of longer residence time.

Both spray granulation and spray drying are scaleable technologies and provide the means for producing bulk quantities of nanophase composite powders at low manufacturing cost.

A direct current plasma fluidized bed was applied to the granulation of spheroidal alloy grains from

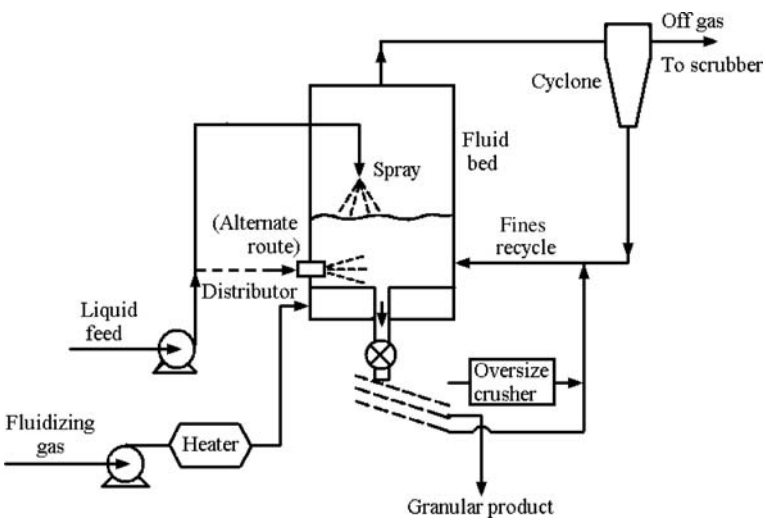

Figure 5.49 Fluidized bed spray granulator. (Source: Ref 113®)

metal powder mixtures [114]. From a mixture of aluminum powder (74–88 μm and 125–149 μm) and iron powder (149–210 μm), alloy grains from 1 to 5 mm in diameter were produced. The grains exhibited a dense homogeneous core and a porous non-homogenous shell structure.

A fluidized bed process facilitates the production of contamination free pyrophoric rare earths and abrasive ceramic powders [115]. The production of exactly limited particle fractions is an important process for rare earths (Sm–Co, Nd–Fe–B) and ceramic oxide (oxides, carbides, nitrides, and borides) products.

Spray Drying

Spray drying is a powder production process in which a slurry or a solution is atomized into droplets in a chamber through which heated gases, usually air, are passed. A typical spray dryer utilizes a disc atomized with co-current air flow. This process is described in Chapter 11.

Spray drying offers several advantages over other powder-processing techniques, particularly in applications requiring agglomerates for subsequent pressing and sintering operations. Spray drying also is one of the most economical ways of drying slurries.

Control of Powder Properties

Most of the applications of spray drying in the metal industry require the formation of free-flowing agglomerates, including the powder injection molding process. Many of these powders are used for producing pressed parts. Therefore, the agglomerate size distribution and bulk density are the two most important properties of spray-dried powders. Agglomeration is achieved by using a binder.

Agglomerate size distribution is a function of atomization conditions and properties of slurry. Commonly, a lower solids content yields a finer average agglomerate size. The maximum attainable solids content varies with material, but usually can be increased by using deflocculating or suspending agents.

Bulk density is a function of the solids content of the slurry additives. Lower bulk densities are generally achieved from slurries with low solids contents. Also, excessive inlet temperatures can cause lower bulk densities. Rapid evaporation of the liquids causes the partially dried droplets to expand rapidly, thus decreasing density. Introduction of frothing agents may draw air into the slurry, which also leads to lower bulk densities. Typically, frothing agents are not added in metallurgical applications.

Moisture content of a powder can be controlled by the inlet and outlet temperature of the spray dryer in conjunction with the slurry feed rate. Moisture levels below 0.1% are possible. For a given airflow and inlet temperature, outlet temperature is controlled by the rate of slurry feed and the solids content. With higher percentages of solids, less water will be evaporated, which leads to higher throughput of dry product.

Binders for agglomeration. Suitable binder materials must be homogeneously dispersable (preferably soluble) in the liquid introduced to form the slurry. When dry, binders must form a coating and/or adhere to the material being agglomerated. They must impart the required strength and crush resistance to the granule for subsequent handling. In addition to the liquid, solids and binders used to formulate a slurry, various other additives may be necessary. Table 5.6 includes typical components of spray-dried slurries.

Plasticizers may be used with binding materials that are hard and that tend to crack during drying. Suspending agents may be needed to prevent solids

Table 5.6 Binders for agglomeration of spray drying slurries

Binder classification	Binder
Organic binders	Polyvinyl alcohol, gum arabic, other natural gums, carboxy-methyl cellulose salts, polyvinyl acetate, methyl cellulose, ethyl cellulose, polyvinyl butyral dispersions, protein colloids, acrylic resin emulsion, ethylene oxide polymers, water-soluble phenolics, lignin sulfonates, propylene glycol alginates, flour, starches
Inorganic binders	Sodium silicate, boric acid, borax, carbonates, nitrates, oxylates, oxychlorides
Plasticizers	Glycerine, ethylene glycol, triathylene glycol, dibutyl phthalate, ethanolamines, propylene glycol, glycenol monochlorhydrin, polyoxyethylene arylether
Deflocculating agents	Sodium hexametaphosphate, sodium molybdenate, tetrasodium pyrophosphate, ammonium citrate, ammonium oxalate, ammonium tartrate, ammonium chloride, monoethylamine
Wetting agents	Synthetic detergents, alkylaryl sulfonates, alkylaryl sulfates, soaps

from settling within the slurry. Deflocculating agents aid the formation of slurries by preventing the agglomeration of fine particles. Wetting agents also may be used to maintain solids in suspension. Some slurries have a tendency to foam during mixing. Antifoaming agents or defoamers may be used to control this action. Chemical activators also may be used as additives to aid in subsequent sintering or processing of powders.

Water Granulation

Water granulation is a process for producing metal granules by pouring molten metals through a screen into water or by agitating molten metals into droplets with subsequent water quenching. Granulation of liquid metal offers a simple technique for solidification of metals, but pouring of liquid metal into water has always been regarded as hazardous. In order to prevent the steam explosion and ignition and explosion of reactive metals like aluminum, a large water tank must be used.

Atomization Techniques

The following conventional atomization processes are used to atomize slurries for spray drying:

- Melt drop orifice atomization
- Centrifugal (rotating disk) atomization
- Two fluid jets atomization.

Table 5.7 includes data about the range sizes of powders produced by the above atomization processes

Table 5.7 The range sizes of powders produced by several atomization processes

Atomization method	Average agglomerate size (μm)
Centrifugal atomization (rotating disk)	
High speed	25–100
Medium speed	50–200
Low speed	100–300
Melt drop orifice atomization	
High pressure	25–100
Medium pressure	50–200
Low pressure	100–300
Very low pressure	200–600
Two fluid jets atomization	
High pressure	10–50
Medium pressure	25–100
Low pressure	50–200

[116]. As shown, the largest agglomerate sizes (600 μm) are achieved by the melt drop orifice atomization. However, recently, this agglomerate size level has been raised up to 2 and 4 mm by using the impulse atomization method [107]. The subsection Melt Drop Orifice Technique in this chapter (p. 213) contains a description of this method, and other paragraphs include the description of centrifugal (rotating disk) atomization and two fluid jets atomization.

Applications

Spray drying applications include production of cemented carbides, mineral processing, production of oxide-dispersion-strengthened alloys and production of powders for thermal spraying applications.

Closed-cycle spray drying is required for most cemented carbide powders because the binders that are used are soluble only in volatile organic fluids. The nitrogen drying gas that is used in the spray drying of cemented carbides is heated to 75–100°C. Viscosity of milled slurries is sometimes modified with stabilizers such as stearic acid (0.3–0.5 wt%). Pressures for melt drop orifice atomization ranges from 590 to 1470 kPa. More detailed description of this is given in Chapter 21.

Multicomponent oxide powders for plasma spraying is an other area of spray drying. The concept of multicomponent powders consists of two steps. The first step is the agglomeration of the starting powder by the drying process. The second step involves plasma densification [117,118]. The plasma densified powder obtained has a spheroidal, smooth surface, a high density and a porosity approaching zero. Experience in this technique concerning the plasma densification of metals, metallic hard materials and ceramics shows that the multicomponent powder concept is practicable for nearly all materials. It has been shown that coatings of plasma densified powders reveal better resistance to wear than coatings of agglomerated powders.

References

1. Dunkley, J.J., Atomization of metals – craft or science? In *Proceedings of 2nd International Conference on Spray Deposition and Melt Atomization*. Bremen Universität, 2003, pp. 3–11.
2. Hopkins, W.G., Hot gas atomization. *European Congress and Exhibition on Powder Metallurgy*, Vol. 4. European Powder Metallurgy Association, 2001, pp. 194–200.
3. Dunkley, J.J., Atomization. In *ASM Handbook*, Vol 7, *Powder Metal Technologies and Applications*. ASM International Publishers, 1998, pp. 35–52.

4. Neikov, O.D., Vasilieva, G.I., Sameljuk, A.V., Krajnikov, A.V., Water atomized aluminium alloy powders. *Materials Science and Engineering* A, 2004, 383:7–13.
5. Seki, Y., Takigava, H., Kawai, N., Effect of atomization variables on powder characteristics. *Met. Powder Rep*., January 1990:38–40.
6. Kikukawa, M., Matsunaga, S., Inaba, T., Iwatsu, O., Takeda, T., Development of spherical fine powders by high-pressure water atomization using swirl water jet. In *Proceedings of 2000 Powder Metallurgy World Congress*. Japan Society of Powder and Powder Metallurgy, Kyoto, 2000, pp. 363–366.
7. Terai, S., Kikukava, M., Inaba, T., Koyata, T., Development of spherical fine powders by high-pressure water atomization using swirl water jet. In *Proceedings of 2006 Powder Metallurgy World Congress*. Korean Powder Metallurgy Institute, 2006, pp. 18–19.
8. Russian Federation Patent 1,812,731, May 1990.
9. Grandzol, R.J., Tallmadge, J.A., Water jet atomization of molten steel. *Am. Inst. Chem. Engineers* J., 1973, 19(6):1149–1158.
10. Klar, E., Fesko, J., On the particle shape of atomized metal powders. *Prog. Powder Metall.*, 1981, 37:47–66.
11. Grandzol, R.J., Tallmadge, J.A., Effect of jet angle of water atomization. *Int. J. Powder Metall. Powder Technol.*, 1975, 11(2):103–116.
12. Lawley, A., *Atomization*. Metal Powder Industries Federation Publishers, Princeton, 2003.
13. Dunkley, J.J., The production of metal powders by water atomization. *Powder Metall. Int.*, 1978, 10(1):38–41.
14. Seki, Y., Okamoto, H., Takigava, H., Kavai, N., Effect of atomization variables on powder characteristics in the high-pressure water atomization process. *Met. Powder Rep.*, 1990, 45(1):38–45.
15. Small, S., Bruce, T.J., The comparison of characteristics of water and inert gas atomized powders. *Int. J. Powder Metall.*, 1968, 4(3):7.
16. Dunkley, J.J., *Atomization of Metal Powders in Powder Metallurgy.* Institute of Metals Publishers, 1991.
17. Levis, G.C. et al., Atomization of liquids in high velocity gas streams. *Ind. Eng. Chem.*, 1948, 40(1):67–74.
18. Yule, A.J., Dunkley, J.J., *Atomization of Melts*. Oxford University Press, 1994.
19. Beddov, J.K., *The Production of Metal Powders by Atomization*. Heyden Press Publishers, Philadelphia, 1978.
20. Sanin, A.F., Nichiporenko, O.S., Influence of water pressure on the powder particle shape during atomization. *Powder Metallurgy and Metal Ceramics,* 1988, 10:1–8.
21. Neikov, O.D., Krajnikov, A.V., Milman, Yu.V. et al., Advanced PM aluminium alloys produced by new rapid solidification technology. In *Proc. PM 2004 World Congress*, European Powder Metallurgy Association, Shrewsbury, UK, 2004, Vol. 1, pp. 237–242.
22. Neikov, O.D., Milman, Yu.V., Sirko, A.I., Sameljuk, A.V., Krajnikov, A.V., Elevated temperature aluminium alloys produced by water atomization. *Materials Science and Engineering* A, 2008, 477:80–85.
23. Dunkley, J.J., An assessment of atomization with hydrocarbon. *Met. Powder Rep.*, February 1992, 22–23.
24. Williams, B., Powder metallurgy – a global market review, 13th edn. 1. Article in *International Powder Metallurgy Directory & Yearbook*, 2008/2009, pp 5–14.
25. US Patent 1,659,291, 1917, February 1928.
26. Wiggers, H., Koster, S.,Walzel, P., Experiments to liquid metal atomization with a new prefilming nozzle. In *Proceedings of International Conference on Spray Deposition and Melt Forming*. Bremen Universität, 2000, pp. 569–578.
27. US Patent 6,481, 638, November 2002.
28. Schulz, G., Concepts for a continuous operation of a WIDEFLOW gas atomizer. In *Proceedings of 2nd International Conference on Spray Deposition and Melt Atomization*. Bremen Universität, 2003, 2, pp. 59–66.
29. Caccioppoli, G., Clausen, B., Bonjour, Ch., Hofman, H., Ultrasonic atomization of metallic melts: modelling and case studies. In *Proc. PM 2004 World Congress, European Powder Metallurgy Association*, Shrewsbury, UK, 2004, Vol. 1, pp. 59–64.
30. Sparchez, Z., Development of new procedures and devices for ultrasonic gas atomization of metallic melts using specific methods of engineering creativity. In *Proc. PM 2004 World Congress, European Powder Metallurgy Association*, UK, 2004, Vol. 1, pp. 25–32.
31. Ünal, A., Flow separation and liquid rundown in a gas atomization process. *Metall. Trans.* B., 1989, 20B(10):613–621.
32. Ünal, A., Influence of nozzle geometry in gas atomization of rapidly solidified aluminium alloy. *Mater. Sci. Technol.*, 1988, 4:909–915.
33. Stobik, M., Nanoval atomizing – superior flow design for finer powder. In *Proceedings of International Conference on Spray Deposition and Melt Atomization.* Bremen Universität, 2000, pp. 511–520.
34. Germany Patent DE 102 37 213.6, August 2002.
35. Achelis, L., Uhlenwinkel, V., Characterization of metal powders generated by pressure-gas-atomizer. *Materials Science and Engineering* A, 2008, 477:60–65.

36. Crisch, C., Fritsching, U., Nozzle design for viscous melt atomization. *Materials Science and Engineering* A, 2008, 477:70–75.
37. Tornberg, C. Gas efficiency in different atomization system. In *Proceedings 'Powder production and spray forming'*, Vol. 1, Metal Powder Industries Federation, 1992, pp. 127–135
38. Dombrovski, N., Johns, W.R., The aerodynamic instability and disintegration of viscous liquid sheets. *Chem Eng. Sci.*, 1963, 18:203–214.
39. Bradley, D., On the atomization of a liquid by high velocity gases: I. *J. Phys. D: Appl. Phys.*, 1973, 6:1724–1736.
40. Bradley, D., On the atomization of a liquid by high velocity gases: II. *J. Phys. D: Appl. Phys.*, 1973, 6:2267–2272.
41. Allen, T., *Particle Size Measurement*, 3rd edn, Chapman and Hall Publishers, 1981.
42. See, J.B., Johnston, G.H., Interactions between nitrogen jets and liquid lead and tin streams. *Powder Tech.*, 1978, 21:119–125.
43. Ingebo, R.D., Capillary and acceleration wave breakup of liquid lets in axial-flow airstreams. NASA Technical Paper 1791, National Aeronautics and Space Administration, Scientific Technical Information Branch, 1981.
44. Sheichaliev, Sh.M., Sharonov, I.V., Karpov, M. P., Centrifugal-hydraulic method of powder production. *Sov. Powder Metall. Met. Ceram.*, 1989, 6:16–21.
45. Ternovoy, Yu.F., Pashetneva, N.N., Manegin, Yu.V., Physicomathematical model of the process of gas spraying of the melt jet. *Sov. Powder Metall. Met. Ceram.*, 1992, (3):11–15.
46. Levich, V.G., *Physicochemical Hydrodynamics.* Phizmatgiz Publishers, Moscow, 1958 (in Russian).
47. Mates, S.P., Biancaniello, F.S., Ridder, S.D., An alternative view of close-coupled gas atomization of liquid metals. In *Proc. 2002 World Congress of PM & Particulate Mater. Metal Powder Ind. Fed.*, Princeton, NJ, 2002, 3, pp. 178–187.
48. Lagutkin, S., Uhlenwinkel, V., Achelis, L., Pulbere, S., Sheikhaliev, Sh., Centrifugal – gas atomization: preliminary investigation of the method. In *Proceedings of PM 2004 World Congress*, European Powder Metallurgy Association, 2004, Vol. 1, pp. 71–76.
49. Klar, E., Fesko, J.W., Atomization. In *Metals Handbook*, Vol. 7, 9th edn., American Society for Metals Publishers, Metals Park, OH, 1984 pp. 25–51.
50. Ünal, A., Effect of processing variables on particle size in gas atomization of rapidly solidified aluminium powders. *Materials Science and Technology*, 1987, 3:1029–1039.
51. Mates, S.P., Ridder, S.D., Biancaniello, F.S., Comparison of the supersonic length and dynamic pressure characteristics of discrete-jet and annular close-coupled nozzles used to produce fine metal powders. In *Proc. Liquid Metal Atomization: Fundamentals and Practice*, The Minerals, Metals, and Materials Society, Warrendale, PA, 2000, pp. 71–81.
52. Ting, J., Peretti, M.W., Eisen, W.B., Control of fine powder production and melt flow rate using gas dynamics. In *Proc. Advances in Powder Metallurgy and Particulate Materials 2000*, Metal Powder Ind. Fed., Princeton, NJ, 2000, 2, pp. 27–40.
53. Anderson, I.E., Terpsta, R.I., Figliola, R., Gas recirculation flow in the melt feeding zone of a close-coupled gas atomization nozzle: modelling and measurement. In *Proceedings of 2nd International Conference on Spray Deposition and Melt Atomization.* Bremen Universität, 2003, 2, pp. 19–30.
54. Anderson, I.E., Figliola, R., Terpsta, R.I., Rau, S., Rauscher, B., Progress in experimental analysis of gas atomization process physics. In *Proc. 2002 World Congress of PM & Particulate Mater.* Metal Powder Ind. Fed., Princeton, NJ, 2002, 3, pp. 150–162.
55. Ünal, R., Effect of the pressure formation at the tip of the melt delivery tube in close-coupled nozzles in gas atomization process. In *Proceedings of 2006 Powder Metallurgy World Congress*, Korean Powder Metallurgy Institute, Busan, Korea, 2006, pp. 562–563.
56. Klar, E., Shafer, W.M., High-pressure gas atomization of metals. *Powder Metallurgy for High-Performance Applications*. Syracuse University Press, Syracuse, NY, 1972.
57. Rai, G., Lavernia, E., Grant, N.J., Powder size distribution in ultrasonic gas atomization. *J. Met.*, 1985, 37(8):22–29.
58. Lubanska, H., Correlation of spray ring data for gas atomization of liquid metals. *J. Met.*, 1970, 22(2):45–49.
59. Wigg, L.D., Drop-size prediction for twin-fluid atomizers. *J. Inst. Fuel*, 1964, (November), 500–505.
60. Dunkley, J.J., Telford, B., Control of 'satellite' particles in gas atomization. In *Proc. 2002 World Congress of PM & Particulate Mater*. Metal Powder Ind. Fed., Princeton, NJ, 2002, 3, pp. 103–110.
61. Nichiporenko, O.S., On the effect of blast energy on the formation process of melt drops during atomization. *Soviet Powder Metall. Ceramics*, 1974, 6:1–7.
62. Rao, P., Tallmadge, J.A., Change of shape of metal droplets in quench atomization. In *Proc. of 1971 Powder Metallurgy Conference*, Metal Powder Industries Federation, 1972, NY, pp. 251–258.

63. Zambon, A., Badan, B., Ramous, E., Gas atomization of nickel aluminide powders. In *Proc. PM 1998 World Congress.* European Powder Metallurgy Association, UK, 1998, Vol. 1, pp. 173–178.
64. Liu, Y., Guo, Sh., Huang, B., Liu, Z., Du, Y., Densification behaviour of Al-Ni-Y powder containing amorphous and nanocrystalline phases. In *Proc. PM 2004 World Congress*, European Powder Metallurgy Association, UK, 2004, Vol. 1, pp. 425–430.
65. L'Estrada, L., Halén, H., Ljunggren, R., Internal porosity of gas atomized powders. In *Proc. Modern Developments in Powder Metallurgy.* Metal Powder Industries Federation, Princeton, NJ, 1988, Vol. 20, pp.187–195.
66. US Patent 5,310,165, May, 1994.
67. German Patent DE 4,102,101 Al, 1991.
68. Pleier, S., Hohmann, M., Goy, W., Schaub, B., Actual improvements of ceramic-free metal powder production. In *Proc. PM 2004 World Congress*. European Powder Metallurgy Association, UK, 2004, Vol. 1, pp. 89–90.
69. Gerling, R., Schimansky, F.P., Crucible- and ceramic-free melting and atomization of Ti-based alloys. In *Proc. PM 2004 World Congress*, European Powder Metallurgy Association, UK, 2004, Vol. 1, pp. 77–82.
70. Yolton, C.F., Gas atomized titanium and titanium aluminide alloys. In *P/M in Aerospace and Defence Technologies*. Metal Powder Industries Federation, Princeton, NJ, 1989. pp. 128–136
71. Babun, A.V., Neklyudov, I.M., Azhazha, V.M., Kovtun, K.V., Vasiliev, A.A., Bobylev, G.G., Beryllium powder metallurgy: developments of the National Scientific Centre 'Kharkov Physicotechnical Institute'. *Powder Metallurgy and Metal Ceramics*, 2006, 3/4:118–125.
72. Wiggers, H., Köster, S., Walzel, P., Experiments to liquid metal atomization with a new prefilming nozzle. In *Proceedings of SDMA 2000 International Conference on Spray Deposition and Melt Atomization*. Bremen Universität, 2000, 2, pp. 569–578.
73. Reichman, S., Chang, D.S., *Superalloys II.* John Wiley & Sons Publishers, 1987.
74. Lierke, E.G., Griesshammer, G., The formation of metal powders by ultrasonic atomization of molten metal. *Ultrasonic*, 1967, 5:224–228.
75. Ruthardt, R., Lierke, E.G., A new ultrasonic atomization technique for the production of metal powder. In *Proc. Modern Developments in Powder Metallurgy*, Metal Powder Industries Federation, Princeton, NJ, 12, 1980, pp. 105–111.
76. Rajan, R., Pandit, A.B., Correlation to predict droplet size in ultrasonic atomization. *Ultrasonics*, 2001, 39:235–255.
77. Lord Rayleigh, *The Theory of Sound*, Vol. II. Dover, NY, 1945.
78. Barreras, F., Amaveda, H., Lozano, A., Transient high-frequency ultrasonic water atomization. *Experiments in Fluids*, 2002, 33:405–413.
79. Yule, A.J., Al-Suleimani, Y., On droplet formation form capillary waves on a vibrating surface. *Proceedings of the Royal Society London, A,* 2000, 456:1069–1085.
80. Al-Suleimani, Y., Yule, A.J. A CFD Prediction of wave development and droplet production on surface under ultrasonic excitation. In *Proc. ILASS-Europe 2002*, 2002, pp. 9–11.
81. Dumouchel, C., Boyaval, S., Use of the maximum entropy formalism to determine drop size distribution characteristics. *Particle and Particle Systems Characterization*, 1999, 16:177–184.
82. Kapur, J.N., Twenty-five years of maximum entropy principle. *Journal Mathematical and Physical Sciences*, 1983, 17:103–156.
83. Dunkley, J.J., Hot gas atomization – economic and engineering aspects. In *Proc. PM 2004 World Congress*, European Powder Metallurgy Association, UK, 2004, Vol. 1, pp. 13–18.
84. Bergmann, H.W., Vetter, J., Cai, Q., Die Erzeugung von Metallpulvern durch Verdüung ihrer Schmelzen mit flüssigen Gasen. *Steels & Met. Mag.*, 1988, 26(10):985–1003.
85. Wolf, G., Nöth, M., Schubert, Martin, V.E., Bergmann, H.W., Production and characterization of liquid gas atomized hard magnetic NdFeB alloy powders for bonded isotropic magnets. *Proc. of the Powd. Met. World Congr.*, 1994, Vol. 3:1745–1753.
86. Wolf, G., Lang, A., Bergmann, H.W., Investigations on melt atomization with gas and liquefied cryogenic gas. In *Proceedings of International Conference on Spray Deposition and Melt Forming*. Bremen Universität, 2000, pp. 535–547.
87. Hinze, H., Milborn, H., Atomization of liquids by means of rotating cup. *J. Appl. Mech.*, 1950, 17(2):145–153.
88. Tanasawa, Y., Miyasaka, Y., Umehara, M., On the filamentation of liquid by means of rotating discs. *J. Japan Mech.* Soc., 1959, 25(156):879–897.
89. Champagne, B., Angers, R., Fabrication of powder by rotating electrode process. *Int. J. Powder Metall. Powder Tech.*, 1980, 16(4):359–364.
90. Champagne, B., Angers, R., REP atomization mechanism. *Powder Metall. Int.*, 1984, 16(3): 125–128.
91. Halada, K., Suga, H., Theoretical investigation on parameters of centrifugal atomization of metal powder. *Powder and Powder Metallurgy*, 1990, 37(4):492–499 (in Japanese).

92. Matsumoto, S., Saito, K., Takashima, Y., Disintegration modes of centrifugal atomization. *J. Eng. Japan,* 1974, 7(1):13–15.
93. Angers, R. et al., Inverted disc centrifugal atomization of 2024. *Int. J. Powder Metall.*, 1994, 30(4):429–434.
94. Dunkley, J.J., Aderhold, D., Centrifugal atomization for powder production. In *Proceedings of International Conference on Spray Deposition and Melt Forming*. Bremen Universität, 2006, pp. 1–6.
95. Superplastic PM superalloys by centrifugal atomization. *Met. Powder Rep.*, 1988, 43(10):688.
96. Bondarev, B.I., Shmakov, Yu.V., *Technology of Rapidly Solidified Al Alloy Production*. All-Russian Institute of Light Alloys Publishers, Moscow, 1997 (in Russian).
97. U.S. Patent 4,343,750, August 10, 1982.
98. Pan, S.V., Slypenyuk, O.M., Kuprin, V.V., Milman, Yu.V., Troy Tacke, V., Influence of scandium concentration on structure peculiarities and hardness of the rapidly-quenched Al–Sc alloys. *Met. Phys. Adv. Tech*., 1999, 18:452–455.
99. Hitoshi, O., Takashi, O., Nobuyki, I., Motonori, N., Development of safe production system for Mg-Zn-Re rapidly solidified powders. In *Proc. PM 2004 World Congress*, European Powder Metallurgy Association, UK, 2004, Vol. 1, pp. 111–115.
100. U.S. Patent 3,099,041, July, 1963.
101. U.S. Patent 3,802,816, April, 1974.
102. Liles, D.T., Deleeuw, D. C., Rapid solidification via centrifugal atomization with a volatile liquid coolant. In *Proc. Rapidly Solidified Crystalline Alloys*. The Metallurgical Society, Warrendale, PA, 1985, p. 285.
103. U.S. Patent 4,347,199, August, 1985.
104. U.S. Patent 4,419,060, December, 1983.
105. Naida, Yu.I., Stepanchuk, A.N., Naida, A.Yu., Industrial production of copper alloys powders using impact atomization method. *Powder Metallurgy and Metal Ceramics*, 2006, 1/2: 112–117.
106. Matei, G., Bicsak, E., Huppmann, W.J., Claussen, N., Atomization of metal powders using the vibrating electrode method. In *Proc. Modern Development in Powder Metallurgy*. Metal Powder Industries Federation, Vol. 9, 1977, pp. 153–160.
107. Henein, H., Impulse atomization: as innovative approach for the generation of powders and spray deposits. In *Proceedings of 2nd International Conference on Spray Deposition and Melt Atomization*. Bremen Universität, 2003, Vol. 1, pp. 31–39.
108. Aldinger, F., Linck, L., Claussen, N., A melt drop technique for the production of high-purity metal powder. *Mod. Dev. P/M,* 1977, 9:141–151.
109. Yim, P. et al., Production and characterisation of mono-sized Sn38Pb alloy balls. *Int. Metall. Powder Technol*, 1996, 32(2):155–164.
110. Kawasaki, A., Watanebe, R., Preparation of monosized spherical particles of metals and alloys by POEM process. In *Proc. 2002 World Congress of PM & Particulate Mater.* Metal Powder Ind. Fed., Princeton, NJ, 2002, 3, pp. 96–102.
111. Singer, A.R.E., Roche, A.D., Roller atomization of molten metals for the production of powder. *Proc. Modern Developments in Powder Metallurgy.* Metal Powder Industries Federation, Princeton, NJ, 1977, 9, p.127.
112. Smagorinski, M.E., Tsantrizos, P.G., Production of spherical titanium powder by plasma atomization. In *Proc. 2002 World Congress of PM & Particulate Mater.* Metal Powder Ind. Fed., Princeton, NJ, 2002, 3, pp. 248–260.
113. Capes, C.E., Particle size enlargement. *Handbook of Powder Technology*. Elsevier Scientific Publishers, 1980.
114. Tsukada, M., Goto, K., Yamamoto, R.H., Horio, M., Metal powder granulation in a plasma-spouted/fluidized bed. *Powder Technol*., 1995, 82(3):347–353.
115. Prem, H., Eddington, D.J., Contamination-free processing of pyrophoric rare earths and abrasive ceramic powders. *Powder Handl. Process.*, 1989, 1(1):101–107.
116. Masters, K., *Spray Drying*, 4th edn. John Wiley & Sons Publishers, 1985.
117. Luo, P., Strutt, P.R., Xiao, T.D., Synthesis of chromium silicide-silicon carbide composite powders. Mater. Sci. Eng. B, 1993, 17(1–3):126–130.
118. Lugscheider, E., Loch, M., Suk, H.G., Powder technology – state of the art. In *Proc. Thermal Spray: Int. Advances in Coatings Technology*. ASM International, 1992, pp. 552–559.

Selected References

Lawley, A., *Atomization*. Metal Powder Industries Federation Publishers, Princeton, 2003.
Dunkley, J.J., Atomization, In *ASM Handbook*, Volume 7, *Powder Metal Technologies and Applications*. ASM International, 1998. pp. 35–52.
Spray drying and granulation. In *ASM Handbook*, Volume 7, *Powder Metal Technologies and Applications*. ASM International, 1998, pp. 91–96.